

REVISED DRAFT  
OPERATION REDWING  
PROJECT 2.2

GAMMA EXPOSURE RATE, VERSUS TIME (U)

RG 338

Location ST. LOUIS FRC  
Access No. 78-0368-Box 1 of 7  
Folder Redwing 2.2  
3-12-10-408 1955-1957-1959

CLASSIFICATION CANCELLED \*  
WITH DELETIONS  
BY AUTHORITY OF DOE/OC  
J. Davis 4/27/92  
REVIEWED BY \_\_\_\_\_ DATE \_\_\_\_\_  
\*CTR DNA SWISHER TO  
DOE/MA-225, 1-23-90  
Kahn 4/27/92

group 1,  
operational  
25 OCT 61 (m)

U.S. ARMY SIGNAL RESEARCH AND DEVELOPMENT LABORATORY  
FORT MONMOUTH, NEW JERSEY

EXEMPT FROM AUTOMATIC DECLASSIFICATION  
DOD DIR 2000.10 DOES NOT APPLY

~~SECRET~~

3R 1210408

B. Fish 27 May 61

~~SECRET~~

[REDACTED]

Copy of [REDACTED]  
[REDACTED]

OPERATION REDWING

WT - 1311

PROJECT 2.2

GAMMA EXPOSURE RATE VERSUS TIME

P. Brown, Project Officer  
G. Carp  
B. Markov  
R. Marnioli

U. S. Army Signal Research and  
Development Laboratory  
Fort Monmouth, New Jersey

February 1959

ST. LOUIS FRC

[REDACTED] RESTRICTED DATA  
[REDACTED]

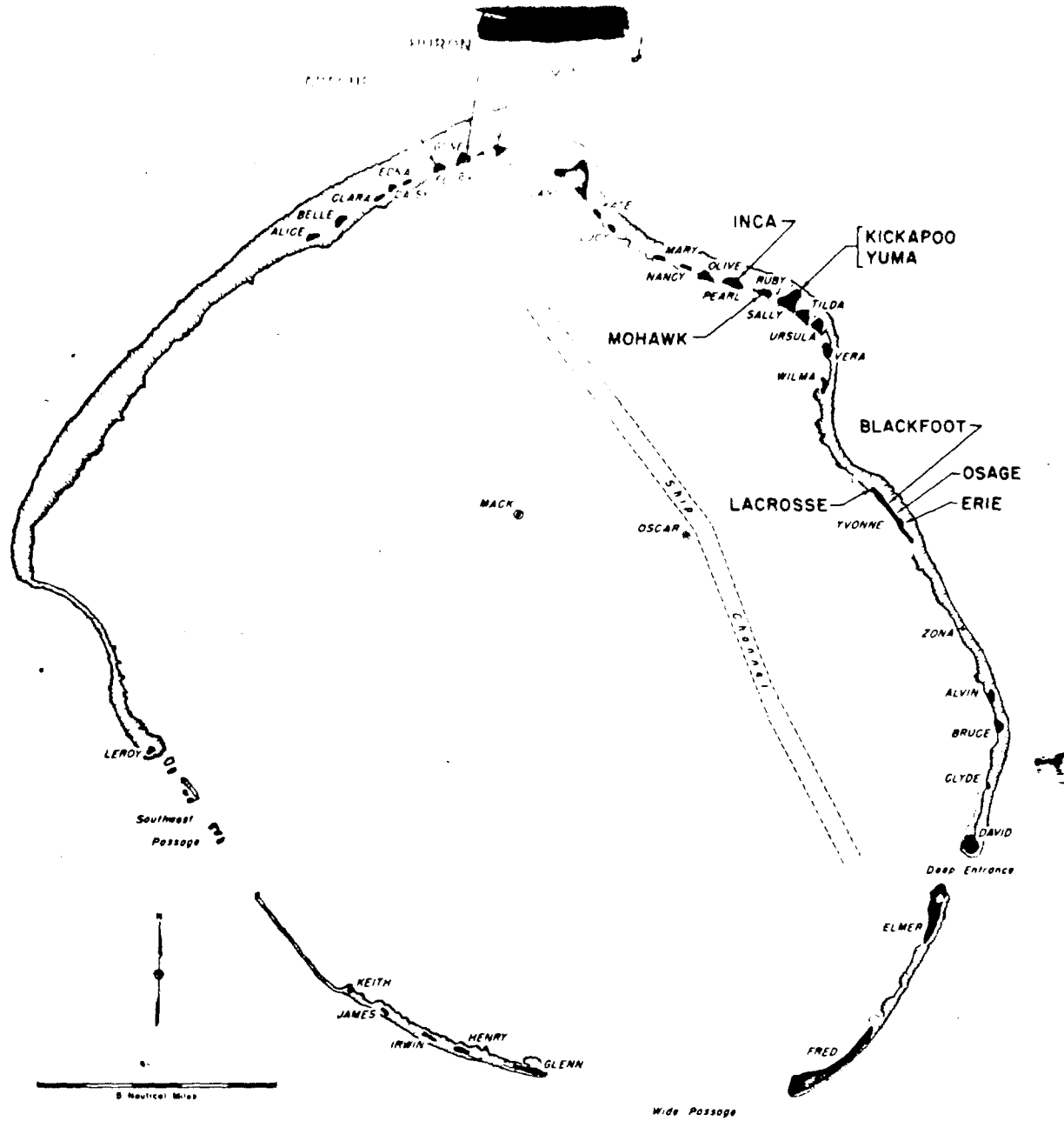
SUMMARY OF SHOT DATA, OPERATION REDWING

Shot Name (Unclassified)	Date (FTG)	Time (Approximate)	Location	Type	HAM Coordinates (Actual Ground Zero)	Geographic
Lacrosse	5 May	0629	Eniwetok Ivonne	Surface Land	124515 E 106885 N	11 33 29 162 21 18
Cherokee	21 May	0551	Bikini Off Charlie	Air Drop (4320:150 ft) Over Water	96200 ± 100 E 185100 ± 500 N	11 43 50 165 19 46
Zuni	28 May	0556	Bikini Tara	Surface Land Water	110909 E 100154 N	11 29 48 165 22 09
Yuma	28 May	0756	Eniwetok Sally	200-ft Tower	112155 E 130604 N	11 37 24 162 19 13
Erie	31 May	0615	Eniwetok Yvonne	300-ft Tower	127930 E 102060 N	11 32 41 162 21 52
Seminole	6 June	1255	Eniwetok Irene	Surface Land <sup>a</sup>	75237 E 149897 E	11 40 35 162 13 02
Flathead	12 June	0626	Bikini Off Dog	Barge Water	115768 E 164094 N	11 40 22 165 23 13
Blackfoot	12 June	0626	Eniwetok Ivonne	200-ft Tower	126030 E 104435 N	11 33 04 162 21 33
Kichipoo	14 June	1126	Eniwetok Sally	300-ft Tower	114018 E 132295 N	11 37 41 162 19 32
Oseage	16 June	1314	Eniwetok Ivonne	Air Drop (680:35 ft) Over Land	126647 ± 50 E 102851 ± 50 N	11 32 48 162 21 39
Inca	22 June	0956	Eniwetok Pearl	200-ft Tower	105300 E 139540 N	11 37 53 162 18 04
Dakota	26 June	0606	Bikini Off Dog	Barge Water	116767 E 164097 N	11 40 22 165 23 13
Nebraska	3 July	0606	Eniwetok Ruby	300-ft Tower	109737 E 132165 N	11 37 39 162 18 49
Apache	9 July	0606	Eniwetok Flora	Barge Water	69227 E 148063 N	11 40 17 162 12 01
Navajo	11 July	0556	Bikini Off Dog	Barge Water	116816 E 160604 N	11 39 48 165 23 14
Tewa	21 July	0546	Bikini Charlie-Dog Reef	Barge Water	99776 E 164476 N	11 40 26 165 20 22
Huron	22 July	0616	Eniwetok Flora	Barge Water	70015 E 148304 N	11 40 19 162 12 09

<sup>a</sup>See ITR-1344 for further details.

RESTRICTED DATA  
ATOMIC ENERGY ACT 1954

W

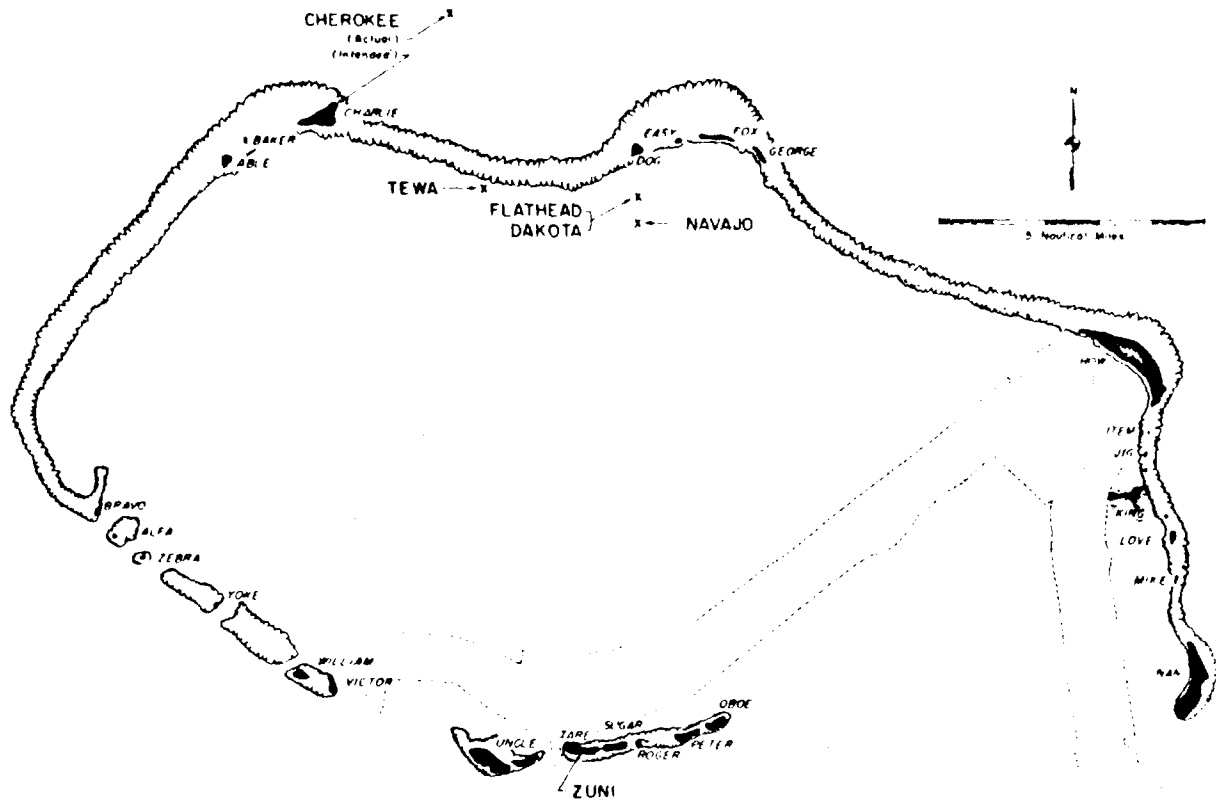


Aaraanbiru	Vera	Chinleero	Alvin	Igurin	Glenn	Ribaion	James
Altau	Olive	Chinimi	Clyde	Japtan	David	Rigiti	Leroy
Antyaanil	Bruce	Cochita	Daisy	Kirinian	Lucy	Rojoa	Ursula
Aomon	Sally	Coral Heads	Mack, Oscar	"M"	Zona	Ruchi	Clara
Bijjiri	Tilda	Eberiru	Ruby	Mui	Henry	Rujoru	Pearl
Bogairikk	Helen	Elugelab	Flora	Muzin	Kate	Runit	Yvonne
Bogallua	Alice	Engebi	Janet	Parry	Elmer	Sandildefonso	Edna
Bogombogo	Belle	Eniwetok	Fred	Piiraal	Wilma	Tetteitripucchi	Gene
Bogon	Irene	Girintin	Keith	Pokon	Irwin	Yeiri	Nancy
Bokonaarappu	Mary						

ST. LOUIS FRC

Eniwetok Atoll. Locations of test detonations during Operation REDWING are indicated by large lettering and arrows. Native island names with corresponding military identifiers are given in the tabulation.

[REDACTED]



Airuki(i)	Oboe	Bokoatokutoku	Alfa	Enirikku	Uncle	Rochikaral	Love
Airukiraru	Peter	Bokobyaadaa	Able	Eninman	Tare	Romurikku	Fox
Aomoen	George	Bokonejien	Baker	Enyu	Nan	Rukoji	Victor
Arrikan	Yoke	Bokonfuaku	Rem	Ionchebi	Mike	Uorikku	Easy
Bigren	Roger	Bokororyuru	Bravo	Namu	Charley	Yomyaran	Jig
Bikini	How	Chieerefe	William	Ourukaen	Zebra	Yurochi	Dog
		Eniatro	King	Reere	Sugar		

ST. LOUIS FRC

Bikini Atoll. Locations of test detonations during Operation REDWING are indicated by large lettering and arrows. Native island names with corresponding military identifiers are given in the tabulation.

[REDACTED]

[REDACTED]

[REDACTED]

ABSTRACT

The primary objective of Project 2.2 was to measure initial- and residual-gamma exposure rates as a function of time at various distances from high-yield thermonuclear detonations. Secondary objectives were: 1) to measure the residual-gamma exposure rate at the lip of the crater from a high-yield land-surface shot, and 2) to field-test a prototype thermal detector to be used in a radiological-defense warning system.

The residual-gamma radiation was detected by an unsaturated ion chamber, whose output determined the frequency of pulses that were recorded on electrosensitive paper. Most of the initial-gamma-radiation stations consisted of scintillation detectors whose output determined the frequency of pulses that were recorded on magnetic tape. Some initial-gamma instruments were similar to those used during Operation Castle. The exposure rate near the crater was measured with a detector-telemeter unit dropped from a helicopter.

Residual-gamma exposure rate versus time was obtained after Shots Zuni, Flathead, Navajo, and Teva. The observed average decay exponents for these events were 1.1 for Zuni and Teva, 1.2 for Flathead, and 1.3 for Navajo. In some cases, the effect of rainfall

ST. LOUIS MO

[REDACTED]

SEARCHED DATE [REDACTED] 1954

~~SECRET~~

in leaching the activity decreased the exposure rate by a factor of two.

Records from Shot Flathead at 7,730 feet and from Shot Navajo at 13,870 feet indicate that at these locations about two-thirds of the total initial-gamma exposure was delivered after the arrival of the shock front.

The crater-lip measurements indicated that the method was a feasible one; however, no usable data was obtained.

The thermal-radiation detector responded satisfactorily to a 5-Mt detonation at a distance of 20 miles.

ST. LOUIS RRC

~~SECRET~~

~~SECRET~~  
54

6

7

[REDACTED]

CONTENTS

ABSTRACT. . . . .	5
CHAPTER 1 INTRODUCTION. . . . .	10
1.1 Objectives. . . . .	10
1.2 Background. . . . .	10
1.3 Theory . . . . .	11
1.3.1 Initial Gamma Radiation . . . . .	12
1.3.2 Residual Gamma Radiation. . . . .	14
1.3.3 Absorption in Air . . . . .	15
1.3.4 Hydrodynamic Effect . . . . .	16
CHAPTER 2 PROCEDURE. . . . .	18
2.1 Operations. . . . .	18
2.2 Instrumentation . . . . .	18
2.2.1 The Residual Instrument System, "Conrad I" Detector. . . . .	20
2.2.2 The Residual Instrument System Recorder. . . . .	22
2.2.3 The Initial Instrument System, "Gustave 1" Detector. . . . .	24
2.2.4 Photomultiplier Feedback Circuit, Initial Instrument System. . . . .	25
2.2.5 Calibration . . . . .	29
2.2.6 High-Range Initial Gamma Station Calibration . . . . .	30
2.3 Readout Error and Accuracy of the Gustave and Conrad Systems. . . . .	29
2.4 Beachball Radiation Detector-Telemeter Unit. . . . .	32
2.5 Thermal-Radiation Detector . . . . .	33
CHAPTER 3 RESULTS AND DISCUSSION . . . . .	34
3.1 Residual Radiation Measurements. . . . .	34
3.1.1 Reliability of the Residual Radiation Data. . . . .	40
3.2 Initial Radiation Measurements . . . . .	40
3.3 Beachball Measurements. . . . .	42
3.4 Thermal-Radiation Detector . . . . .	43
CHAPTER 4 CONCLUSIONS . . . . .	74
4.1 Residual Gamma Exposure Rate. . . . .	74
4.2 Initial Gamma Exposure Rate . . . . .	74
4.3 Beachball Operation. . . . .	75
4.4 Thermal-Radiation Detector . . . . .	75
REFERENCES . . . . .	76

ST. LOUIS RRC



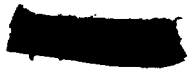
**TABLES**

1.1 Energy Partition in Fission. . . . .12  
 1.2 Calculated Buildup Factors . . . . .16  
 2.1 Shot Participation and Instrumentation . . . . .19  
 3.1 Zuni Instrumentation and Residual-Exposure Information. . . .36  
 3.2 Flathead Instrumentation and Residual-Exposure Information . .37  
 3.3 Navajo Instrumentation and Residual-Exposure Information . . .38  
 3.4 Teva Instrumentation and Residual-Exposure Information. . . .39

**FIGURES**

1.1 Graph of gamma exposure versus distance for a 1-kt surface burst . . . . .13  
 2.1 Schematic diagram showing the basic circuit for the Conrad and Gustave detectors . . . . .21  
 2.2 Graph showing a typical calibration curve for the Conrad detectors. . . . .23  
 2.3 Graph showing typical calibration curves for the Gustave detectors. . . . .20  
 2.4 Energy dependence, Gustave I Detector, normalized to Co<sup>60</sup> energy (1.25 Mev), dose rate 100 r/hr . . . . .27  
 2.5 Schematic diagram showing the photomultiplier feedback circuit of the initial gamma detector system. . . . .28  
 3.1 Residual exposure rate within blast shield vs time, Zuni . . .44  
 3.2 Unshielded residual exposure rate vs time, Zuni . . . . .45  
 3.3 Residual exposure rate vs time, Zuni. . . . .46  
 3.4 Unshielded residual exposure rate vs time, Zuni . . . . .47  
 3.5 Unshielded residual exposure rate vs time, Zuni . . . . .48  
 3.6 Unshielded residual exposure rate vs time, Flathead. . . . .49  
 3.7 Residual exposure rate within blast shield vs time, Flathead. .50  
 3.8 Residual exposure rate within blast shield vs time, Flathead. .51  
 3.9 Residual exposure rate within blast shield vs time, Flathead. .52  
 3.10 Unshielded residual exposure rate vs time, Flathead. . . . .53  
 3.11 Unshielded residual exposure rate vs time, Flathead. . . . .54  
 3.12 Unshielded residual exposure rate vs time, Navajo . . . . .55  
 3.13 Residual exposure rate within blast shield vs time, Navajo . .56  
 3.14 Residual exposure rate within blast shield vs time, Navajo . .57  
 3.15 Residual exposure rate within blast shield vs time, Navajo . .58  
 3.16 Residual exposure rate vs time, Teva. . . . .59  
 3.17 Residual exposure rate within blast shield vs time, Teva . . .60  
 3.18 Residual exposure rate within blast shield vs time, Teva . . .61  
 3.19 Map of Bikini Atoll showing unshielded residual exposures for Shot Zuni. . . . .62  
 3.20 Map of Bikini Atoll showing unshielded residual exposures for Shot Flathead . . . . .63  
 3.21 Map of Bikini Atoll showing unshielded residual exposures for Shot Navajo . . . . .64  
 3.22 Map of Bikini Atoll showing unshielded residual exposures for Shot Teva. . . . .65





FIGURES - continued -

3.23	Shielded initial exposure rate vs time, Zuni. . . . .	.66
3.24	Shielded initial exposure rate vs time, Flathead . . . . .	.67
3.25	Shielded initial exposure rate within blast shield vs time, Navajo . . . . .	.68
3.26	Shielded initial exposure vs time, Zuni . . . . .	.69
3.27	Shielded initial exposure vs time, Flathead . . . . .	.70
3.28	Shielded initial exposure vs time, Navajo. . . . .	.71
3.29	Shielded initial exposure vs time, Projects 2.1 and 2.2, Zuni	.72
3.30	Shielded initial exposure vs time, Projects 2.1 and 2.2, Flathead and Navajo . . . . .	.73

ST. LOUIS FRC



~~SECRET~~

CHAPTER 1  
INTRODUCTION

1.1 OBJECTIVES

The primary objectives of Project 2.2 were: 1) to measure the initial-gamma exposure rate as a function of time from the detonation of high-yield thermonuclear devices; and 2) to measure the residual-gamma exposure rate as a function of time at land fallout stations. Secondary objectives were: 1) to measure residual radiation at early times on the crater lip of a high-yield land-surface shot; and 2) to field-test a prototype thermal-radiation detector to be used in a radiological-defense warning system.

1.2 BACKGROUND

Los Alamos Scientific Laboratory (LASL) measured initial-gamma exposure rate versus time for high-yield devices during Operation Ivy (Reference 1). It was found that high-yield devices did not follow the relatively simple scaling laws of low-yield devices. Gamma radiation at a particular distance scales linearly with yield for devices up to about 100 kt. For megaton-range devices, gamma radiation scales higher with increasing yield. This enhancement of initial-gamma radiation was attributed largely to the hydrodynamic effect (Section 1.3.4). U. S. Army Signal Research and Development Laboratory (USASRDL) obtained several gamma-exposure-rate-versus-time data points from high-yield devices during Operation Castle (Reference 2). The

~~SECRET~~

~~CONFIDENTIAL~~  
1954

//

~~SECRET~~

data obtained by USASFDL were lower by a factor of 10 or more than the Super-Effects Handbook predictions (Reference 3).

One of the purposes of Project 2.2 was to resolve the initial-gamma radiation scaling laws for high-yield devices. Of particular interest was a high-yield airburst, since it would allow correlation of the hydrodynamic effect from an airburst with that from a surface burst. USASFDL made measurements of residual-gamma exposure rates from high-yield devices during Operation Castle (Reference 2). Only limited data were obtained because of a high loss of instruments early in the operation. These data indicated that the decay exponent for the residual activity varied with the type of nuclear device. Another purpose of Project 2.2 was to determine accurate decay exponents for residual activity.

The thermal-radiation detector, part of an early-warning system for nuclear detonations, was tested with low-yield devices during Operation Teapot (Reference 4). The tests were successful; the detector showed a capability far in excess of the requirements. It was decided to determine the response of this detector to megaton-range devices during Operation Racking in order to complete the testing.

1.3 THEORY

ST. LOUIS FRC

The gamma radiation emitted from a nuclear detonation may be divided into two portions: initial radiation and residual radiation. The residual radiation may include radiation from both fallout and neutron-induced activity.

~~SECRET~~ ACT 1954

//

12

~~SECRET~~

1.3.1 Initial Gamma Radiation. For a fission-type device the initial radiations are divided approximately as shown in Table 1.1 (from Reference 5). The major contribution to initial gamma radiation is from the fission-product gammas and the gamma radiation from neutron capture by  $N^{14}$  ( $n, \gamma$ ) in the HE components and air. The prompt gammas are nearly all absorbed in the device itself and are of little significance outside of the device. The fission-product gammas predominate at close distances (Reference 5). The  $N^{14}$  ( $n, \gamma$ ) gammas become relatively more important at greater distances, and eventually become the major contributor. This applies only to devices with yields of less than 100 kt, in which the hydrodynamic effect is small. Figure 1.1 shows the contribution from fission-product gammas and  $N^{14}$  ( $n, \gamma$ ) for a 1-kt surface burst. With respect to time, the  $N^{14}$  ( $n, \gamma$ ) radiation is essentially emitted within 0.2 seconds; the fission-product gammas, however, continue to contribute for the first 30 seconds.

TABLE 1.1 ENERGY PARTITION IN FISSION  
(Reference 5)

Mechanism	Percent of Total Fission Energy	Total Energy per Fission
	percent	Mev ST. LOUIS PRC
Kinetic Energy of Fission Fragments	81	162
Prompt Neutrons	4	8
Prompt Gammas	4	8
Fission Product Gammas	2.7	5.4
Fission Product Betas	2.7	5.4
Fission Product Neutrinos	5.5	11
Delayed Neutrons	0.2	0.2
Totals	100.0	200.0

\*Mostly absorbed in the device.

~~SECRET~~

~~SECRET~~ OCT 1954

~~SECRET~~

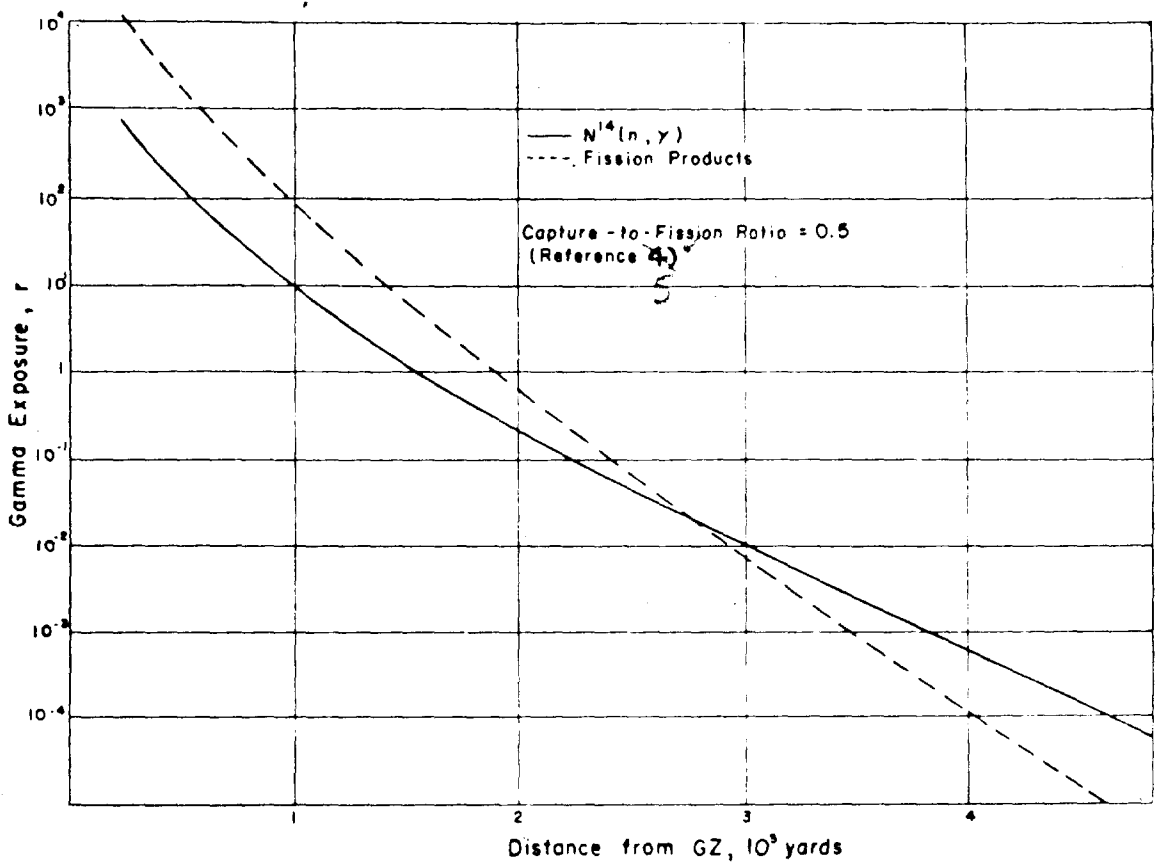


Figure 1.1 Graph of gamma exposure versus distance for a 1-kt surface burst. This illustration shows the contribution from fission-product gammas.

ST. LOUIS MRC

~~SECRET~~

~~SECRET~~



For thermonuclear devices, in addition to gamma radiation from fission-product gammas, it is necessary to consider the interaction of neutrons from the fusion process with  $N^{14}$ . The radiation due to the fusion process may vary over wide limits, depending on the design of the device. For a given yield, the number of neutrons available may be ten times as great for fusion as for fission, and therefore a large contribution to gamma radiation exposure may be due to the  $N^{14}$  (n,  $\gamma$ ) reaction in a thermonuclear device (Reference 3).

1.3.5 Residual Gamma Radiation. The residual gamma radiation consists of fission-product radiation from fallout and radiation from neutron-induced activity. The decay rate of the residual radiation from fallout will follow approximately the expressions:

$$I_t = I_1 t^{-1.2} \tag{1.1}$$

and:

$$r = \int_{t_1}^{t_2} I_t dt = 5I_1 (t_1^{-0.2} - t_2^{-0.2})$$

- where:  $I_t$  = exposure rate at time  $t$ .
- $I_1$  = exposure rate at unit time.
- $t$  = time.
- $r$  = exposure between times  $t_1$  and  $t_2$ , where
- $t_1 \geq 10$  seconds.

ST. LOUIS SRC

The decay of the residual radiation is expected to vary with weapon design. For example, the presence of  $U^{235}$  would tend to decrease the absolute value of the decay exponent for a period of time.



~~SECRET~~

1.3.3 Absorption in Air. The absorption of unscattered gamma radiation in air is exponential with distance. From a point source of monoenergetic radiation, the variation of intensity with distance is expressed as:

$$I_D = I_0 e^{-\mu D} / 4\pi D^2 \quad (1.2)$$

where:  $I_D$  = intensity at distance D

$I_0$  = source intensity

$\mu$  = total linear absorption coefficient (this coefficient generally decreases with increasing gamma energy)

D = distance

The absorption coefficient  $\mu$  in Equation 1.2 is applicable for narrow-beam geometry, and a correction should be made for field conditions where the detector is approximately a 4 $\pi$  sensing element. This is done by adding a buildup factor B to Equation 1.2 to account for the scattered radiation that will be detected. Buildup factors for different energies and distances have been calculated (Reference 6), and some values are shown in Table 1.2. For omnidirectional detectors, the expression is:

$$I_D = I_0 B e^{-\mu D} / 4\pi D^2 \quad (1.3)$$

ST. LOUIS, MO

~~SECRET~~

~~SECRET~~

FORM 1954

~~XXXXXXXXXX~~

TABLE 1.2 CALCULATED BUILDUP FACTORS

The buildup factor (B) given here is the factor  $B_{\Sigma}(\mu_0 D, E_0)$  as computed by Nuclear Development Associates for AFSWF (Reference 6).

Energy ( $E_0$ )	B		
	1000 yds	1500 yds	3000 yds
1 Mev			
1	16.2	29.3	85.0
3	3.65	5.35	10.2
4	2.97	4.00	7.00
10	1.70	2.01	2.90

1.3.4 Hydrodynamic Effect. As shown in Section 1.3.3, the attenuation of gamma radiation is highly dependent on the amount of absorber between the source and the detector. For weapons of less than 100-kt yield, essentially all of the initial gamma radiation is emitted before the shock front can produce an appreciable change in the effective absorption of the air between source and detector. For high-yield devices, the velocity of the shock front is sufficiently high to produce a strong enhancement of a large percentage of the initial gamma radiation (Reference 7). The higher the yield, the larger is this percentage. A simplified treatment of the hydrodynamic effect follows.

Assume a sphere that has a volume  $V_0$  and radius  $R$ , and is filled with a gas of density  $\rho_0$  and mass  $M$ . Then,

$$M = V_0 \rho_0 = \frac{4\pi R^3 \rho_0}{3} \tag{1.4}$$

ST. LOUIS PRO

Let the gas be compressed into a shell with thickness  $\Delta R$





CHAPTER 2

PROCEDURE

2.1 OPERATIONS

Table 2.1 gives the shot participation and instrumentation. The instrument stations were placed in the previously prepared positions at the latest practicable time prior to each shot, and were recovered post-shot as soon as Red-Safe conditions permitted. The residual stations were activated upon placement. Their 5-day operating period allowed for 2 days of data-recording and three 1-day shot delays. For the surface bursts, the initial stations were activated by a minus-1-minute timing signal for warmup, and a minus-15-second signal to start the recording. Shot Zuni was an exception; only a minus-1-second signal was available to start the recorder. Timing signals were necessary on the initial stations due to the limited recording time available (Cook Research Laboratory MR 33 recorders, 4 minutes; Sanborn recorders, 15 minutes). For Shot Cherokee, the recorders were not started until after the bomb release.

2.2 INSTRUMENTATION

In designing the instrumentation for this project, there were two objectives: (1) to design the instruments so as to best fulfill the requirements; and (2) to design flexible instruments readily adaptable to a wide variety of field measurements. In view of this dual objective, the instruments were designed to be compact, drift-free, reliable, wide in dynamic-range coverage, and low in cost. The basic circuit evolved measures discrete increments of charge. Essentially, this circuit may be used with any sensing element that has an output which is a known function of the radiation field. Thus, the circuit is equally applicable

TABLE 2.1 SHOT PARTICIPATION AND INSTRUMENTATION

Shot	Station		Range from Ground Zero ft	Instrumentation
	Number	Location		
Cherokee	221.01	Able	29,400	Ip,Ig,R
	221.02	Charlie	20,694	Ip,Ig,R
	221.03	Dog	16,370	R
	221.04	Easy	20,062	R
	221.05	Fox	24,922	R
	221.06	George	30,207	R
	220.01C	Uncle	85,432	R
	220.08C	Oboe	76,310	R
	221.02C	Yoke	63,720	R
	Portable	Nan		R
Zuni	221.03	Dog	68,600	R
	221.06	George	70,900	R
	220.01C	Uncle	10,300	R
	220.08C	Oboe	16,270	Ip,R
	220.09C	Roger	7,000	Ip,Ig,R
	220.14C	Peter	11,270	R
	221.01C	William	10,320	R
	221.02C	Yoke	43,400	R
	221.04	Alfa	56,570	R
	Portable	How	78,000	R
	Portable	Love	72,000	R
	Portable	Nan	69,000	R
	Flathead	221.01	Able	45,800
221.03		Dog	4,422	Ip,Ig,R
221.04		Easy	7,730	Ip,Ig,R
221.05		Fox	10,745	Ip,R
221.06		George	14,920	R
220.08C		Oboe	59,880	R
220.09C		Roger	63,155	R
220.14C		Peter	62,344	R
221.01C		William	40,907	R
221.02C		Yoke	9,068	R
221.04C		Alfa	70,000	R
Portable		How	60,000	R
Portable		Love	75,000	R
Portable		Nan	85,000	R
Navajo		221.01	Able	46,000
	221.03	Dog	7,922	Ip,Ig,R
	221.04	Easy	10,700	Ip,R
	221.05	Fox	13,170	Ig,R
	221.06	George	16,180	Ig,R
	220.08C	Oboe	56,341	R
	220.01C	Uncle	58,282	R
	221.01C	William	36,006	R
	221.02C	Yoke	15,582	R
	Portable	How	60,000	R
	Portable	Love	72,000	R
	Portable	Nan	84,000	R
	Tewa	221.01	Able	28,950
221.03		Dog	17,550	Ip,Ig,R
221.04		Easy	22,200	R
221.05		Fox	24,711	R
220.08C		Oboe	54,966	R
		42	5,960	Ig
221.01C		William	51,775	R
221.02C		Yoke	37,641	R
Portable	How	70,000	R	

Ig = initial station, Gustave  
 Ip = initial station, Photomultiplier  
 R = Residual station

ST. LOUIS, MO

~~RESTRICTED DATA~~  
 ACT 1954

to ion chambers, scintillation detectors, or photoconductive crystals.

See Figure 2.1. In operation, the charge on  $C_1$  holds tube  $T_1$  well beyond cutoff. The output current of the sensing element discharges  $C_1$  at a rate dependent upon the radiation level. When the voltage at the grid of  $T_1$  reaches the grid base,  $T_1$  conducts, feeds a negative signal to the grid of  $T_2$ , and initiates a regenerative action which rapidly cuts  $T_2$ . Then  $C_1$  charges to a potential equal to B-plus less the cathode voltage and the grid-to-cathode drop through the diode action of the grid of  $T_1$ . When  $C_1$  is completely charged, the circuit returns to its normal condition of  $T_2$  conducting and  $T_1$  cutoff. The circuit will remain in this condition until  $C_1$  is once more discharged by the output of the sensing element. The output of this circuit consists of pulses that have a repetition rate proportional to the output current of the sensing element.

2.2.1 The Residual Instrument System. "Conrad I" Detector. In general, decay of the gamma-exposure rate from fallout contamination is given by:

$$I = I_1 e^{-\lambda t} \tag{2.1}$$

where:  $I$  = the gamma-exposure rate at time  $t$

$I_1$  = the gamma-exposure rate at unit time

$\lambda$  = the decay constant (given as 1.2 for gross fission products)

Measurements of the decay constant require good (short) time resolution at early times ( $t$  small,  $I$  large) when the changes in gamma-exposure rate are most rapid. At later times ( $t$  large,  $I$  small), the rate of change of the gamma-exposure rate of the gamma radiation is much smaller, and the instrument system need not have such good time resolution. The instrument for the measurement of residual-gamma

~~SECRET~~

~~CONFIDENTIAL~~

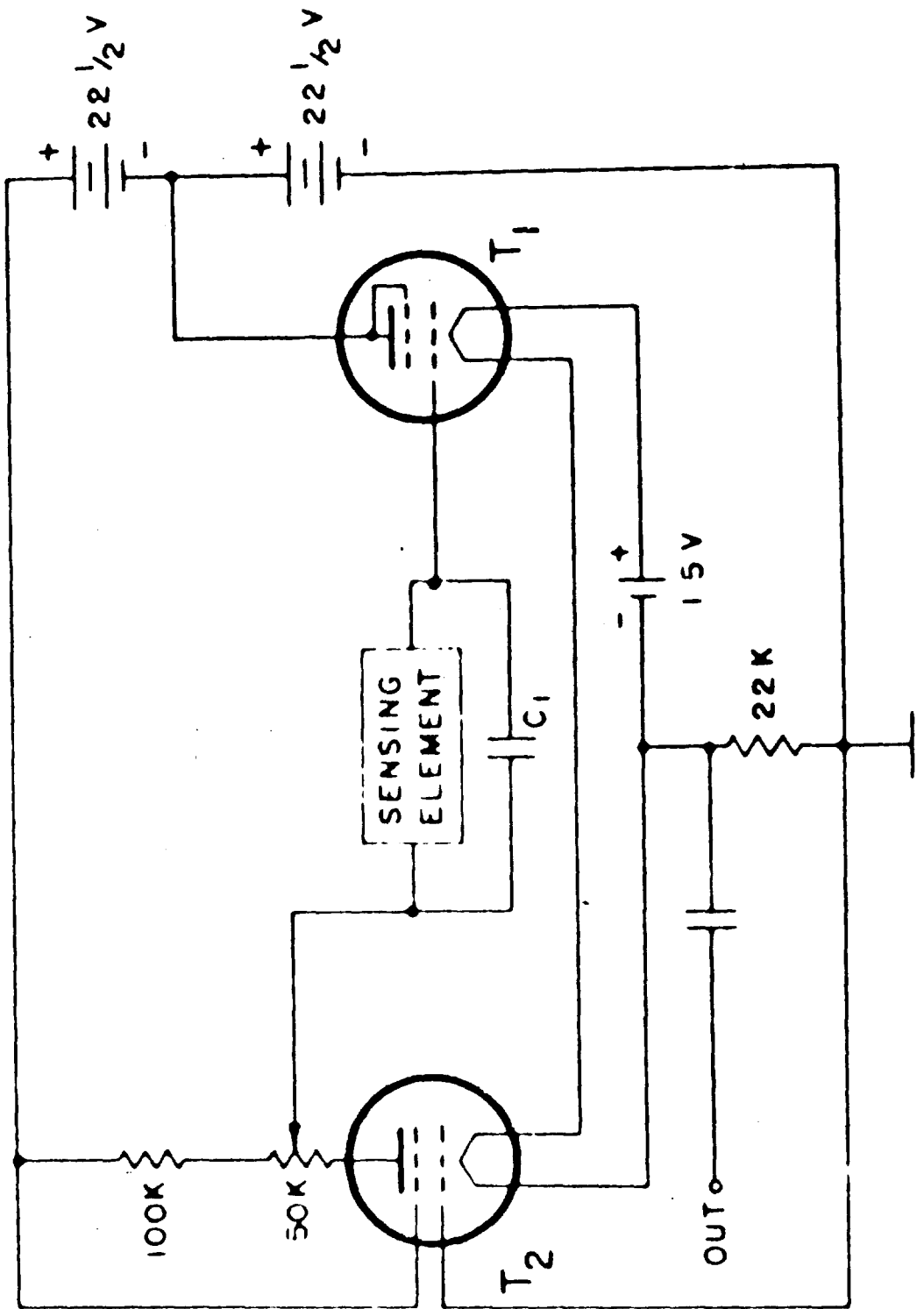


Figure 2.1 Schematic diagram showing the basic circuit for the Conrad and Gustave detectors. The Conrad detector used an unsaturated ion chamber as the sensing element, whereas the Gustave detector used a scintillation detector.

ST. LOUIS MO

~~RESTRICTED BY ATOMIC ENERGY ACT 1954~~



radiation is designed to cover a range from 1 r/hr with a time resolution of 5 minutes, to  $10^4$  r/hr with a time resolution of 0.05 minutes. The basic circuit is shown in Figure 2.1, where the sensing element is an unsaturated ion chamber. The ion chamber was designed to have a current output proportional to the square root of the gamma-exposure rate. The overall detector response is given by:

$$f = kr^{1/2} \tag{2.2}$$

where:  $f$  = the output frequency

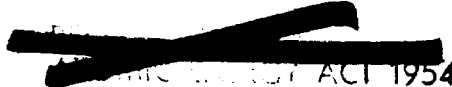
$r$  = the gamma-exposure rate in r/hr

$k$  = a parameter chosen to meet specific design objectives

In laboratory calibrations on a 250-kv X-ray beam, these detectors have shown a precision of better than 2 percent, including drift effects, over a three-week period. The completed detector head, including ion chamber and electronics, was encapsulated in Eysol 6000 casting resin. A typical calibration curve for these detectors is given in Figure 2.2.

2.2.2 The Residual Instrument System Recorder. The two-channel recorder used with this system consisted of an Esterline-Angus chart drive to supply the time base and two electric styluses writing on Teledeltos paper charts. The output from the detector head was fed through an amplifier directly to Stylus Number 1, which produced a mark for each detector output pulse. In addition, the detector output was fed to a scale-of-11 counter, thence to Stylus Number 2. Thus, Stylus 2 produced one mark for each 11 output pulses from the detector. In this manner, a chart-speed slow enough for the required 5-day operating period could be used while maintaining resolution of the fastest

ST. LOUIS ARC



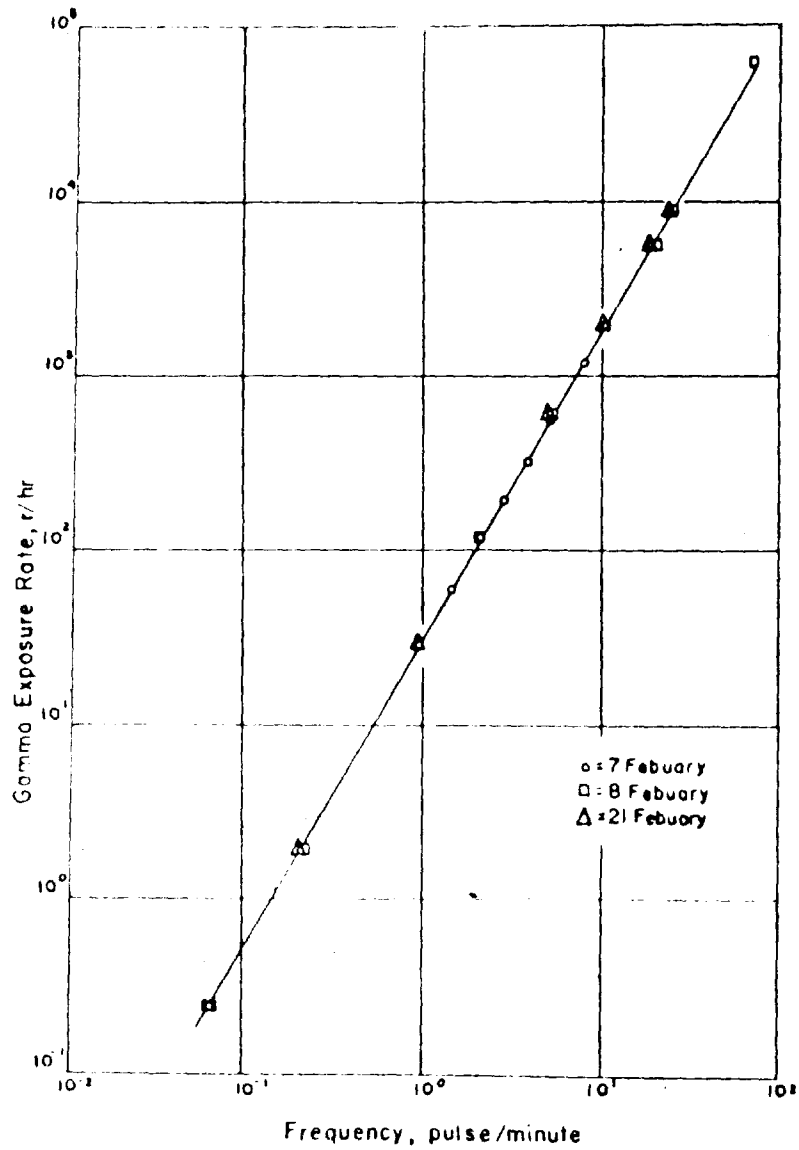


Figure 2.2 Graph showing a typical calibration curve for the Conrad detectors. These detectors were calibrated with the 200-curie  $Co^{60}$  source and the 250-kv xray generator.

ST. LOUIS ERC

~~RESTRICTED BY ATOMIC ENERGY ACT 1954~~

~~SECRET~~

anticipated pulse-repetition rate. In operation, the record from Stylus 1 was used until the pulse-repetition rate was so great that the recorded marks overlapped and could not be resolved. At that time, Stylus 2 could be used, each mark representing 11 pulses from the detector head. The chart drive that supplied the time base was calibrated with a Watchmaster before each event. By means of the Watchmaster, the chart drive could be set to have a maximum error of 1 minute in 24 hours, or  $\pm 0.069$  percent. This is not the optimum recording system for use with this detector, but rather a compromise forced by a lack of funds and time.

2.2.3 The Initial Instrument System, "Gustave I" Detector. For the high-range, fast-resolution detector, the basic circuit of Figure 2.1 was used with a scintillation detector as the sensing element. The latter consisted of an RCA 929 phototube and a National Radiac Scintillation Board plastic photomultiplier in a electron-equilibrium thickness of bakelite to provide an air-equivalent response (Reference 8). The electron-equilibrium layer presents a source of electrons that may be scattered into the crystal to replace those electrons produced by radiation absorbed near the crystal surfaces and lost without being detected. These detectors were constructed to cover three ranges,  $10^2$  to  $10^6$  r/hr,  $10^3$  to  $10^7$  r/hr, and  $10^4$  to  $10^8$  r/hr. The overall detector response is given approximately by:

$$f = kr \quad (2.3)$$

where:  $f$  = the pulse repetition rate

$r$  = the gamma-exposure rate in r/hr

$k$  = a parameter chosen to meet specific design objectives

ST. LOUIS ERC

[REDACTED]

The maximum pulse-repetition rate of these instruments is 1,000 pulses/sec, the maximum rate that may be resolved by the recorder (a Cook Research Laboratory MR-33 eight-channel magnetic-tape recorder). Typical calibrations for these detectors are shown in Figure 2.3. Figure 2.4 shows the energy dependence of the Scintillon-phosphor Gustave I detector, relative to Co<sup>60</sup> gamma radiation at a rate of 100 r/hr. To reduce the errors due to flutter and wow, a 1,000-cycle time base was recorded on the tape simultaneously with the gamma-exposure-rate data. An American Time Products transistorized frequency standard with an accuracy of 10.02 percent was used to provide the time base.

2.2.4 Photomultiplier Feedback Circuit. Initial Instrument System.

This system is essentially the same as that used during Operation Cassile (Reference 2). The detecting element, a Scintillon phosphor 2.75 inches in diameter by 0.5 inches in height mounted in a bakelite block for electron equilibrium, was placed inside a blast-resistant housing at the top of a light pipe. The output of the crystal after passing through the light pipe was detected by an RCA 6199 photomultiplier tube. The photomultiplier tube was used in a 100-percent-feedback circuit which held the photomultiplier tube anode current nearly constant, regardless of the incident light flux, by reducing the dynode voltage (Figure 2.5). The gain of a photomultiplier tube with constant anode current is approximately proportional to the antilog of the dynode voltage. In this manner, a useful dynamic range of about a factor of 10<sup>7</sup> was realized.

ST. LOUIS AEC

[REDACTED]

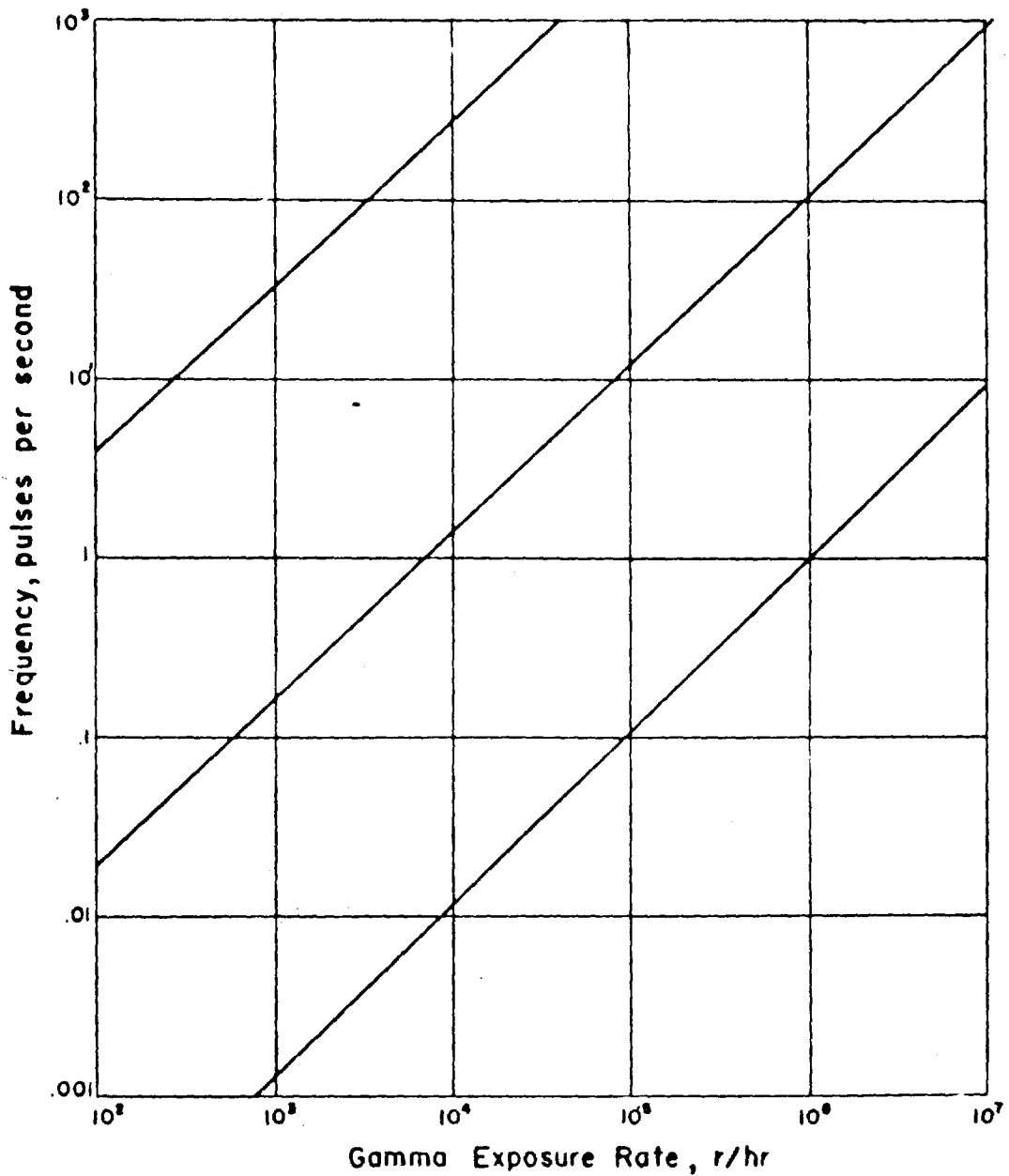


Figure 2.3 Graph showing typical calibration curves for the exposure detectors. These detectors were calibrated with the 200- $\mu$  x-ray generator and the 2.0-Mev Van de Graaff generator.

ST. LOUIS FRC

~~RESTRICTED DATA~~

~~SECRET~~

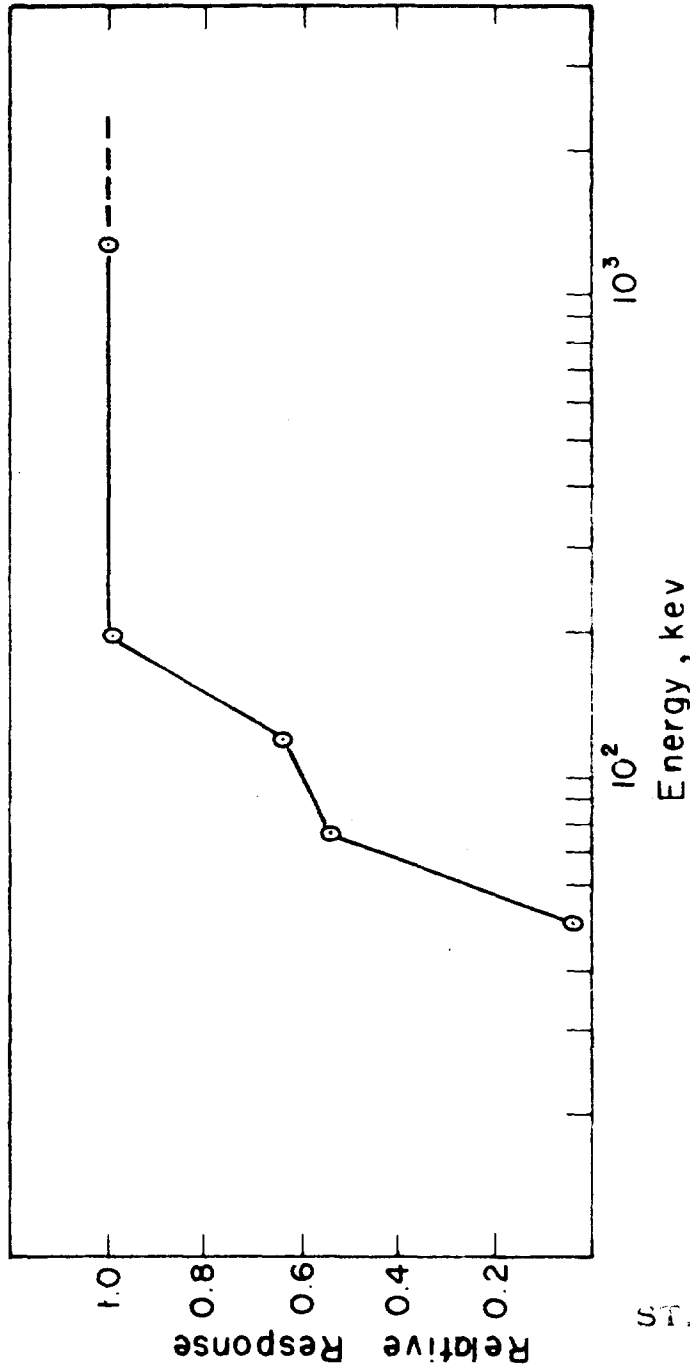


Figure 2.4 Energy dependence of Gustave I detector normalized to Co<sup>60</sup> energy (1.25 Mev), dose rate 100 r/hr.

CONFIDENTIAL

~~RESTRICTED DATA ACT 1957~~

IA

~~CONFIDENTIAL~~

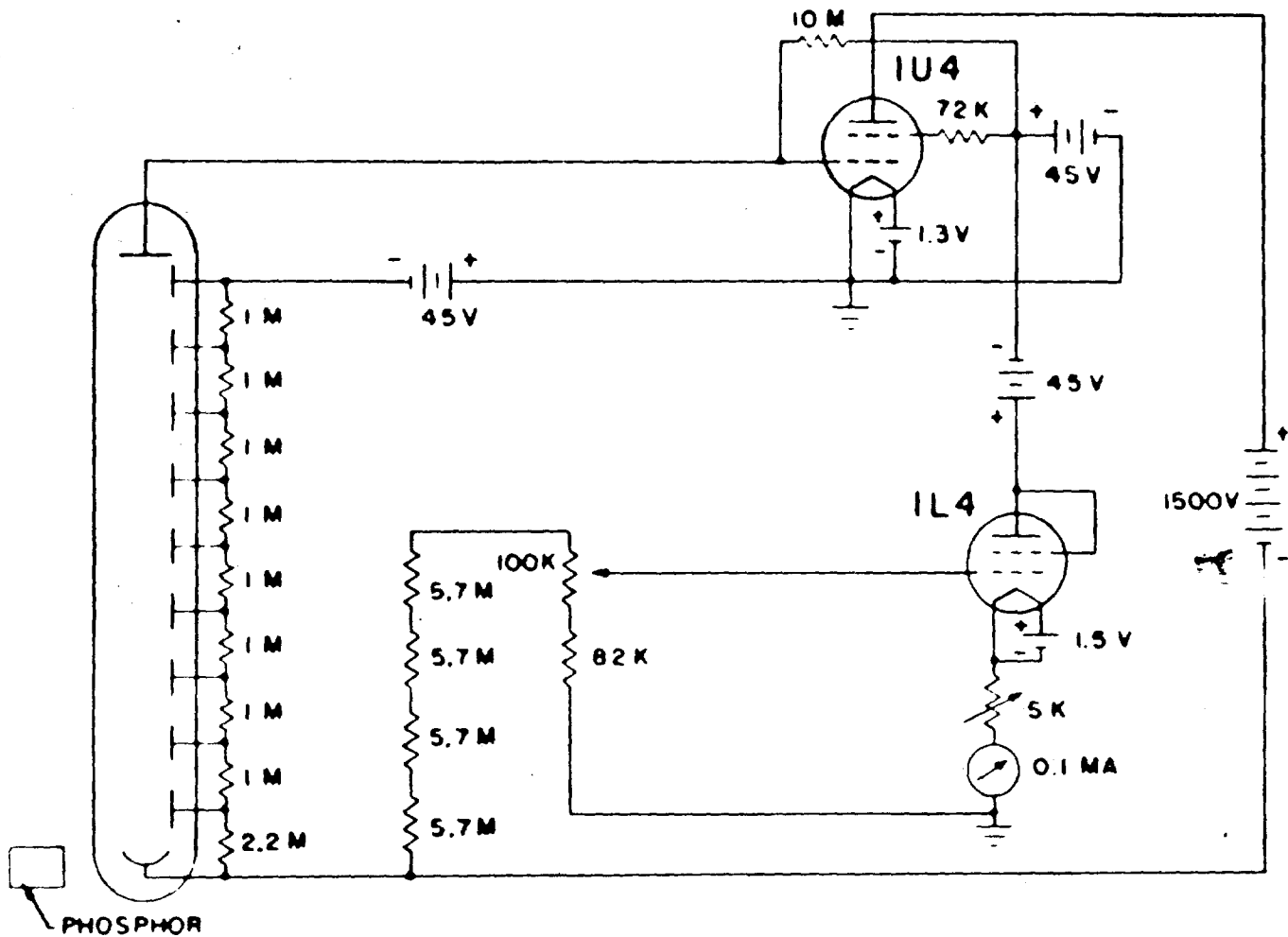


Figure 2.5 Schematic diagram showing the photomultiplier feedback circuit of the initial-gamma detector system.

ST. LOUIS ERC

RESTRICTED DATA

1954

~~SECRET~~

2.2.5 Calibration. Three radiation sources, a 250-kv Xray generator, a 2.5-Mev Van de Graaff generator, and a 200-curie Co<sup>60</sup> source were used in the calibration of the Project 2.2 instruments. The "Conrad" detectors were calibrated with the 200-curie Co<sup>60</sup> source and the 250-kv Xray generator. The initial gamma instruments, the "Gustaves" and the photomultiplier feedback circuit detectors, were calibrated with the 250-kv Xray and the 2.5-Mev Van de Graaff generator.

The 250-kv Xray machine was operated at an applied potential of 250 kv, and 10-ma current. The Xray beam was hardened with 1 mm of cadmium filtration to give an effective energy of 190 kev. The instrument response to this beam was the same as for Co<sup>60</sup>, since the instrument response is flat to below 125 kev. The maximum usable exposure rate attainable with this Xray generator (consistent with good geometry) was 6,400 r/hr.

The Van de Graaff generator was operated at 1.0, 1.5, and 2.0 Mev, resulting in a maximum rate of 10<sup>6</sup> r/hr.

The 200-curie field calibrator was specifically designed for operation under EPG weather conditions. The main components are the source container and the control trailer. The source container is made of stainless steel, and the plug and rise tube assembly of Monel metal. The source, inclosed in a double-walled Monel capsule, is raised and lowered pneumatically and is supported by three spring-loaded pins, one of which actuates a microswitch to indicate when the source is up.

The Co<sup>60</sup> is in pellet form and fills a space 0.39 inches in diameter and 1.98 inches in length. The total Monel metal shielding (capsules and rise tube) is 0.33 inches. The source was calibrated in the field over

ST. LOUIS FRC

~~SECRET~~ ~~RESTRICTED AREA~~ 54

[REDACTED]

the exposure rate region used with a set of Victoreen  $\pi$ -meters calibrated at National Bureau of Standards (NBS) in March 1956.

2.2.6 High-Range Initial Gamma Station Calibration. There were no sources available for direct gamma-radiation calibration up to the maximum ranges of the initial gamma instruments. Because of this lack, scintillation detectors were used, thereby enabling calibration with a light source. In practice, the instruments were directly calibrated by the use of the 200-curie  $\text{Co}^{60}$  source in the field and a Van de Graaff generator in the laboratory to the limit of the available radiation rates. The calibration was then extended to the maximum range through the use of a light calibration, which was normalized to the radiation calibration.

The light calibrator consists of a light source filtered to provide a beam having approximately the same spectral quality as the light output of the scintillator, and a series of neutral density filters that vary the light output in known discrete steps. Errors due to the direct response of the circuit elements to gamma radiation are introduced into the calibration; however, these errors have been shown to be small in the ranges where the light and radiation calibrations overlap. There are no reasons why the relative error should increase beyond the range of dual calibration.

ST. LOUIS FRC

### 2.3 READOUT ERROR AND ACCURACY OF THE GUSTAVE AND CONRAD SYSTEMS

In general, the output of the Gustave and Conrad detectors may be given as:

$$x = kt^n \quad (2.4)$$

[REDACTED]

[REDACTED]

where:  $r$  = gamma exposure rate

$t$  = time between output pulses

$n, k$  = design parameters

If the error in reading time between pulses (i.e. time base) is  $\Delta t$ ,

then:

$$\begin{aligned}r + \Delta r &= k(t + \Delta t)^n \\ \Delta r &= k[(t + \Delta t)^n - t^n] \\ \frac{\Delta r}{r} &= \frac{(t + \Delta t)^n - t^n}{t^n}\end{aligned}\tag{2.5}$$

For  $\frac{\Delta t}{t} \ll 1$ , this formula reduces to the definition of differentials.

$$\frac{\Delta r}{r} \doteq \frac{n \Delta t}{t}\tag{2.6}$$

where:  $\frac{\Delta r}{r}$  = the relative error in gamma exposure rate due to errors in the time measurement

$\frac{\Delta t}{t}$  = the relative time measurement error

For the Conrad I detector,  $n = -2$ , and:

$$\frac{\Delta r}{r} \doteq \frac{-2 \Delta t}{t}\tag{2.7}$$

In practice, at high-pulse-repetition rates, a number of pulses  $N$  over a period  $T$  was used to read out the data. Hence, from equation 2.5:

$$\begin{aligned}\frac{\Delta r}{r} &\doteq \frac{(Nt + \Delta t)^n - (Nt)^n}{(Nt)^n} \\ \frac{\Delta r}{r} &\doteq \frac{(T + \Delta t)^n - (T)^n}{T^n} \\ &\doteq \frac{n \Delta t}{T}\end{aligned}\tag{2.8}$$

ST. LOUIS CRC

where:  $\Delta t$  now includes all errors in reading the time interval  $T$ .

~~SECRET~~

The time-base error for the Conrad recorders was  $\pm 0.069$  percent; therefore, the readout error was negligible, and the errors of the Conrad I system (of the order of 10 percent) could be attributed to the detector itself.

For the Gustave I system,  $n = -1$ , and:

$$\frac{\Delta K}{K} = -\frac{\Delta t}{t} \quad (2.9)$$

Hence the Gustave I system error was essentially that of the detector (the time-base error  $\pm 0.02$  percent), and was of the order of 10 percent.

#### 2.4 BEACHBALL RADIATION DETECTOR-TELEMETER UNIT

To attain the objective of measuring the residual-exposure rate on the crater of a land-surface burst, a droppable radiation detector-telemeter unit was devised. A Gustave I detector system was connected to key a 1/2-watt VHF transmitter that had been constructed in the field. The detector and transmitter were mounted in a polyethylene bottle suspended at the center of an air-inflated, 5-foot, plastic beachball. The beachball was attached to a 27-pound lead brick by means of a 6-foot line. This made it possible to drop the system from a helicopter more accurately with a minimum of impact shock to the instrumentation. The lead brick hit the ground first and allowed the beachball to slow down over the 6-foot distance before hitting the ground. In addition, the beachball itself acted as a good impact absorber. Once the beachball was released, the helicopter could go a short distance away and orbit in a radiologically safe region, while receiving the data transmitted from the beachball unit.

ST. LOUIS RRC

~~SECRET~~

~~SECRET~~  
ENERGY ACT 1954

~~SECRET~~

## 2.5 THERMAL-RADIATION DETECTOR

The thermal-radiation detector consists of a phototube, amplifier, and high and low band-pass filters. The phototube output is produced by incident thermal radiation from a nuclear device, lightning strokes, or other sources. This output is fed to a high band-pass filter that passes only signals with a rise time similar to those due to nuclear detonations, and to a low band-pass filter that passes only those signals with a duration typical of nuclear detonations. Thus, an incident thermal-radiation signal must have both a rise time and a duration typical of nuclear devices in order to activate the thermal-radiation detector.

72

ST. LOUIS MO

~~SECRET~~

~~RESTRICTED DATA  
ALL INFORMATION CONTAINED  
HEREIN IS UNCLASSIFIED~~

~~SECRET~~

### CHAPTER 3

#### RESULTS AND DISCUSSION

##### 3.1 RESIDUAL RADIATION MEASUREMENTS

The data obtained from the residual radiation stations are shown in Figures 3.1 through 3.18 in the form of log-log plots for convenience of presentation and for ease of determination of the decay exponent. The decay exponent is equal to the slope of a straight line drawn through the data points that are considered to be related to each other only by radioactive decay. All residual data was analyzed in detail for this report; the instruments for those stations represented by Figures 3.3, 3.11, and 3.12 were operating at levels below their high-resolution region and did not yield the essentially continuous curves shown in the remainder of the group of Figures 3.1 through 3.18. On Figures 3.1 through 3.18 the slopes are shown as dashed lines which were drawn through the linear portion of the curves. In drawing these dashed lines, early times were avoided when the concentration of gamma-ray sources was still building up because of continuing deposition of fallout material, and other data points were ignored in cases where rain or wind had redistributed the fallout material and caused perturbations in the decay curve.

ST. LOUIS FRC

Measured residual gamma radiation doses for each of the four shots are plotted on maps of Bikini Atoll in Figures 3.19 through 3.22. Free-field exposures shown on these figures were extrapolated to infinite time using Equation 1.2, Section 1.3.2, of this report.

~~SECRET~~

~~RESTRICTED DATA  
ALL INFORMATION CONTAINED  
HEREIN IS UNCLASSIFIED~~



Tables 3.1 through 3.4 summarize the data on residual station locations, time of arrival of fallout, maximum observed exposure rate, total exposure, and decay exponent. The average decay exponent was found to be 1.1 for Shots Zuni and Teva, 1.3 for Shot Navajo, and 1.2 for Shot Flathead (neglecting the results from Station 221.04C, which received too little exposure for accurate evaluation). In the many cases where there was early rain leaching, the slope indicated by the data points taken after rain had ceased was used to help determine the best-fit straight line. Figures 3.14 and 3.15 are typical curves showing the gamma-exposure-rate change caused by rainfall. In these curves, the gamma-exposure rate after rainfall was approximately half of that expected if the normal radioactive decay were the only cause of change of exposure rate.

In Figures 3.3 and 3.18, the buildup of the exposure rate is apparently more complex than the monotonic buildup presented by most of the other figures. It appears that fallout ceased to arrive for a short period at 60 minutes in Figure 3.18 and then commenced to arrive again.

Slope changes are evident in the curves in Figures 3.9 and 3.10 after about plus 500 minutes. This effect is probably not due to instrumentation errors, because these curves represent the data from two independent instruments located at the same station. A possible explanation of these slope changes is the presence of one (or more than one) radioactive isotope whose half-life is such that the decay is slower than the combined fission fragment decay of  $T^{-1.2}$ , and the decay slope is dominated by this isotope from about plus 500 minutes until the end of the record. However, the instrumentation did not record for a sufficiently long time to determine definitively the half-life of this isotope.

ST. LOUIS RRC

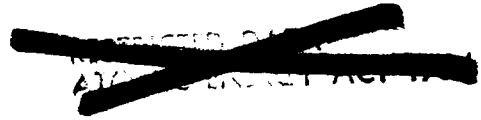


**TABLE 3.1 EMI INTERFEREANCE AND RESIDUAL-EXPOSURE INFORMATION**

<u>Island</u>	<u>Station</u>	<u>Azimuth From QZ</u>	<u>Distance From QZ</u>	<u>Arrival Time</u>	<u>Max Rate<sup>a</sup></u>	<u>Total Exposure<sup>a</sup></u>	<u>Decay Exponent</u>
		degrees	feet	min	r/hr	r	
Dog	221.03	5.5	68,600	27.7	81.2	703(72.9 hr)	1.07
George	221.06	17.1	70,900	31	42	349(77.8 hr)	1.07
How	Portable	60	78,000	28.8	17	126(74.5 hr)	1.04
Uncle	221.01C	268.8	10,300	2.6	28	139(85 hr)	1.1
Yoke	221.02C	292.2	43,400	25.3	80	125(20.4 hr)	1.18
Han	Portable				No fallout		
Charlie	221.02				Drive inoperative		
Love	Portable				Stylus and drive inoperative		
Oboe	220.08C				Drive inoperative		
Peter	220.14C				Stylus inoperative		
Roger	220.09C				Stylus and drive inoperative		
William	221.01C				Drive inoperative		
Alfa	221.04C				Drive inoperative		

ST. LOUIS ARC

<sup>a</sup>Corrected to free-field values

~~SECRET~~

~~CONFIDENTIAL~~  
~~ALCO~~ 1954

~~SECRET~~

**TABLE 3.2 FLATHEAD INSTRUMENTATION AND RESIDUAL-EXPOSURE INFORMATION**

<u>Island</u>	<u>Station</u>	<u>Azimuth From OZ</u>	<u>Distance From OZ</u>	<u>Arrival Time</u>	<u>Max Rate<sup>d</sup></u>	<u>Total Exposure<sup>d</sup></u>	<u>Decay Exponent</u>
		<u>degrees</u>	<u>feet</u>	<u>min</u>	<u>r/hr</u>	<u>r</u>	
Able	221.01	277.3	45,800	44			
Alfa	221.04c	235.6	70,000	41			
Easy	221.04	37.9	7,730	37.5			
Fox	221.05	52.2	10,745	37			
George <sup>a</sup>	221.06	74.5	14,920	42			
George <sup>b</sup>	221.06	74.5	14,920	42			
How	Portable						No fallout
Love	Portable						No fallout
Oboe	220.08c						No fallout
Uncle	220.01c						No fallout
Dog	221.03						Stylus intermittent
Easy	221.04						Stylus inoperative (2nd detector)
Man	Portable						Stylus inoperative
William	221.01c						Drive inoperative
Yoke	221.02c						Drive inoperative

**DELETED**

ST. LOUIS FRC

<sup>a</sup>Detector inside of steel pipe, 0.30-inch wall thickness

<sup>b</sup>Detector outside of steel pipe.

<sup>c</sup>Questionable due to small amount of radiation

<sup>d</sup>Corrected to free-field values

~~SECRET~~

~~RESTRICTED DATA~~

[REDACTED]

TABLE 3.3 NAVAJO INSTRUMENTATION AND RESIDUAL-EXPOSURE INFORMATION

Island	Station	Azimuth From GZ	Distance From GZ	Arrival Time	Max Rate <sup>a</sup>	Total Exposure <sup>a</sup>	Decay Exponent
		degrees	feet	min	r/hr	r	
Able	221.01	281.5	46,300	32.1			
Dog	221.03	0	7,922	31.3			
Easy	221.04	26	10,700	31.2			
Fox	221.05	40	13,170	34			
George	221.06				Drive inoperative		
How	Portable				Drive inoperative		
Love	Portable				Drive inoperative		
Nan	Portable				Drive inoperative		
Obos	220.08C				Drive inoperative		
Uncle	220.01C				Drive inoperative		
William	221.01C				Drive inoperative		
Yoke	221.02C				Drive inoperative		

DELETED

<sup>a</sup>Corrected to free-field values

ST. LOUIS FRC

[REDACTED] 1954

~~SECRET~~

TABLE 3.4 TEWA INSTRUMENTATION AND RESIDUAL-EXPOSURE INFORMATION

Island	Station	Asimuth From GZ	Distance From GZ	Arrival Time	Max Rate <sup>a</sup>	Total Exposure <sup>a</sup>	Decay Exponent
		degrees	feet	min	r/hr	r	
Able	221.01	280.8	28,950	17.5	1,078	4,277(74.8 hr)	1.03
Dog	221.03	76.7	17,550	44.7	140	1,327(55 hr)	1.29
Easy	221.04	75.2	22,220	15.3	105	1,139.6(73 hr)	1.11
Oboe	220.08c		No fallout				
How	Portable		Stylus inoperative				
Fox	221.05		Drive inoperative				
William	221.01c		Drive inoperative				
Yoke	221.02c		Drive inoperative				

<sup>a</sup>Corrected to free-field values

ST. LOUIS WRC

~~SECRET~~

~~RESTRICTED DATA  
ATC 1954~~

[REDACTED]

The initial-gamma-exposure-rate data presented are subject to uncertainty in absolute magnitude. Data reduction indicated a strong possibility that the wiring of the magnetic-tape recorders might not have been the same as previously presumed and that the association of a particular recorder channel with a particular detector sensitivity range might have been incorrect. The wiring could not be checked in the laboratory because the equipment had been disassembled at the termination of the field phase of the operation. Subsequent analysis of the recorded pulse shapes has led to the association assumed for the initial-gamma data presented herein, and the derived total-exposure values agree reasonably well with those measured by Redwing Project 2.1 (Reference 9). However, there is still some uncertainty on this point, and the curves presented may be off in absolute magnitude, although the shape of the curves as a function of time is probably correct.

The initial-gamma values given represent those observed at the detector and should be multiplied by a factor of approximately 1.2 to correct for station shielding. This factor of 1.2 is a measured value of the attenuation of the blast shield for  $Co^{60}$  radiation; the attenuation is a function of the energy of the incident radiation. Time is a factor only in that after one minute there is little gamma radiation in this energy range (> 1 Mv). Figures 3.23 through 3.25 should be multiplied by 1.2 to give free-field values.

ST. LOUIS FRC

The data in Figures 3.26 is in reasonable agreement with similar data in Reference 9, especially after the data of Figure 3.26 has been extrapolated to a time equivalent to that reported by Redwing Project 2.1.

[REDACTED]

~~RESTRICTED DATA~~  
~~APPROPRIATELY CLASSIFIED~~

~~SECRET~~

3.1.1 Reliability of the Residual Radiation Data. In general, the residual instrumentation functioned either very well or not at all. Tables 3.1 through 3.4 show that the major malfunctions were due to inoperative chart drives. The possibility of malfunctioning of the recorders was anticipated prior to the operation; however, lack of funds and time forced the use of these recorders. The recorders that worked were checked with a Timexstar and adjusted to within ±0.069 percent accuracy. The repeated calibrations of the instrument systems indicated a maximum total error of less than 10 percent.

Figures 3.1, 3.3, 3.7, 3.8, 3.9, 3.13, 3.14, 3.15, 3.16, 3.17, and 3.18 present data taken with the detector heads inside a steel pipe, which served as blast and thermal protection. The results from these stations should be increased by a factor of about 1.4 to compensate for the shielding of the blast housings. This estimate of the shielding factor was derived from the field measurements at Station 221.06, Shot Flathead, where one detector was inside and the other was outside the blast housings. On the other hand, Figures 3.2, 3.4, 3.5, 3.6, 3.10, 3.11, and 3.12 present data from detector heads without blast shields. These detectors were calibrated for free-field conditions ( $Co^{60}$ ) and give free-field data.

**3.2 INITIAL RADIATION MEASUREMENTS**

ST. LOUIS RRC

The results from the initial-gamma stations are shown in Figures 3.23, 3.24, and 3.25. The initial-gamma station for Shot Euni (Station 220.09C) was destroyed by the shock wave, and the data from this station are available only to shock arrival and are given in Figure 3.23. Figures 3.26, 3.27, and 3.28 present the total initial-gamma exposure as a function of time.

~~SECRET~~

~~RESTRICTED BY  
ATOMIC ENERGY ACT 1954~~

[REDACTED]

Figures 3.27 and 3.28 show that approximately two-thirds of the total initial exposure for Flathead 221.04 and Navajo 221.05 is delivered after the arrival of the shock front. Most of this exposure is due to the enhancement caused by the hydrodynamic effect, because the exposure rate was decaying rapidly before the arrival of the shock front.

Reference 9 compares measured initial gamma exposure-versus-distance curves with curves computed from TN 23-200. For the purpose of comparison with published data, integrated initial gamma rate data from Figures 3.26, 3.27, and 3.28 of this report have been plotted on the corresponding curves from Reference 9. In addition, extrapolation of Project 2.2 measured data (integrated initial gamma rate) to include initial gamma dose delivered after the end of project records has been made using information and methods in Reference 10. Exposure received prior to start of project records has been neglected, since the exposure is relatively insignificant. The above-mentioned plots for Shot Zuni are shown in Figure 3.29 and for Shots Flathead and Navajo in Figure 3.30.

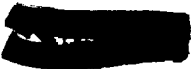
3.3 BEACH-BALL MEASUREMENTS

ST. LOUIS FRC

The objective of measuring the exposure rate at the lip of the crater from Shot Zuni was assumed by Project 2.2 at a late stage in the preparations for Operation Redwing. The beach-ball instrument was dropped onto the Zuni crater lip at H + 6 hours. The fall apparently caused a change in the calibration of the system, because the received data indicated an exposure rate as high as 50,000 r/hr at this late time. Furthermore, rotor interference made reception of the transmitted signal difficult.

[REDACTED]

~~RESTRICTED~~  
~~ATOMIC ENERGY ACT 1954~~



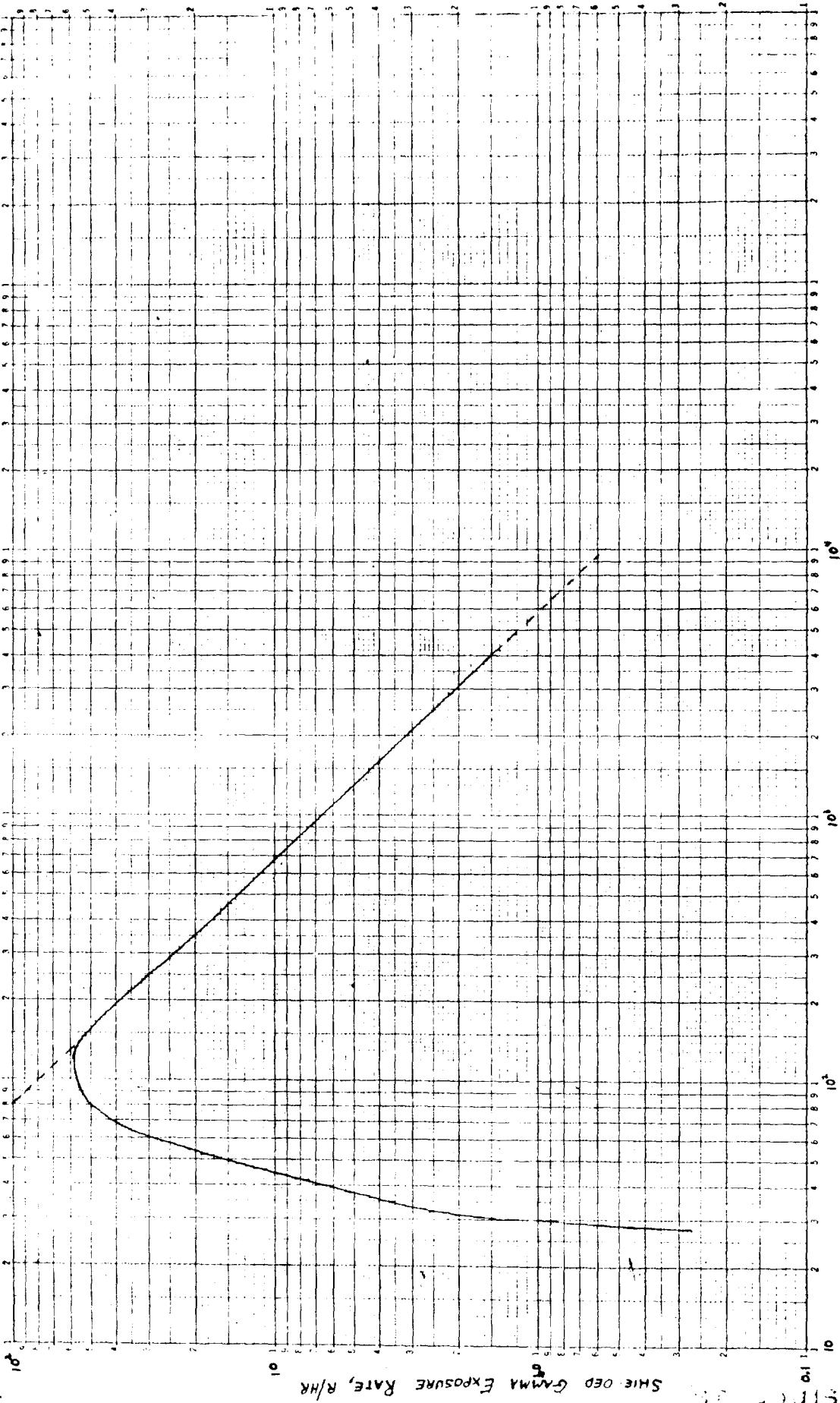
3.4 THERMAL-RADIATION DETECTOR

The thermal-radiation detector was installed on Site Man for Shot Tewa at a range of approximately 20 miles, and the detonation was satisfactorily detected.

ST. LOUIS FRC

7

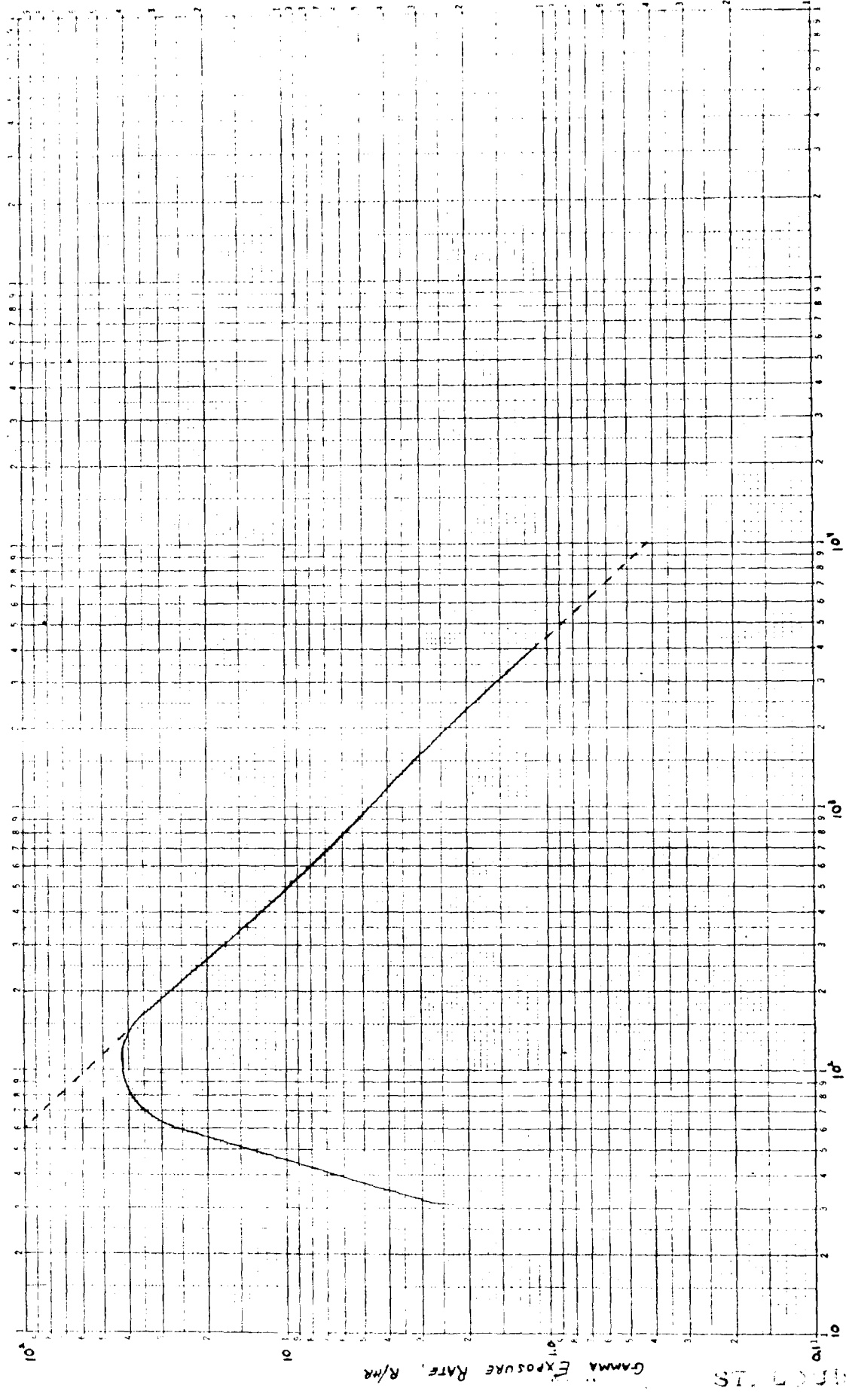
~~RESTRICTED DATA  
ATOMIC ENERGY ACT 1954~~



TIME AFTER SHOT, MINUTES

Figure 3.1 Residual exposure rate within blast shield versus time for Zuni; Station 221.03, range 68,600 feet. For unshielded rate multiply by 1.4. Total 72.9-hour exposure, 502r.

~~RESTRICTED DATA  
ATOMIC ENERGY ACT 1954~~



TIME AFTER SHOT, MINUTES

Figure 3.2. Unshielded residual exposure rate versus time for Zuni; Station 221.06, range 70,900 feet. Total 77.6-hour exposure, 349r.

96

54

~~CONFIDENTIAL~~  
1054

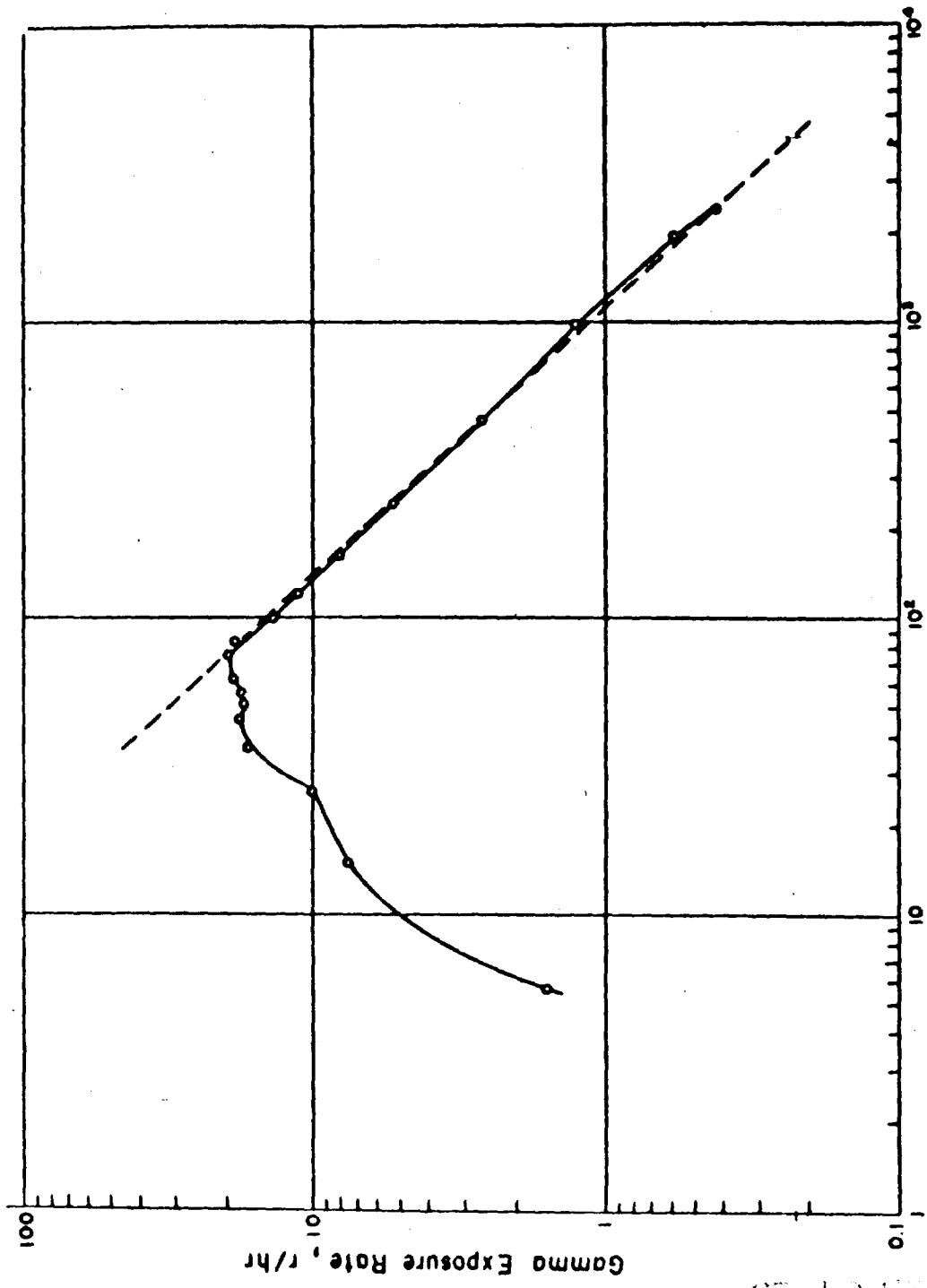


Figure 3.3 Residual exposure rate versus time for Zuni; Station 221.01C, range 10,300 feet. For unshielded rate multiply by 1.45 Total 85-hour exposure, 99 r.

ORNL 1954

~~CONFIDENTIAL 1954~~

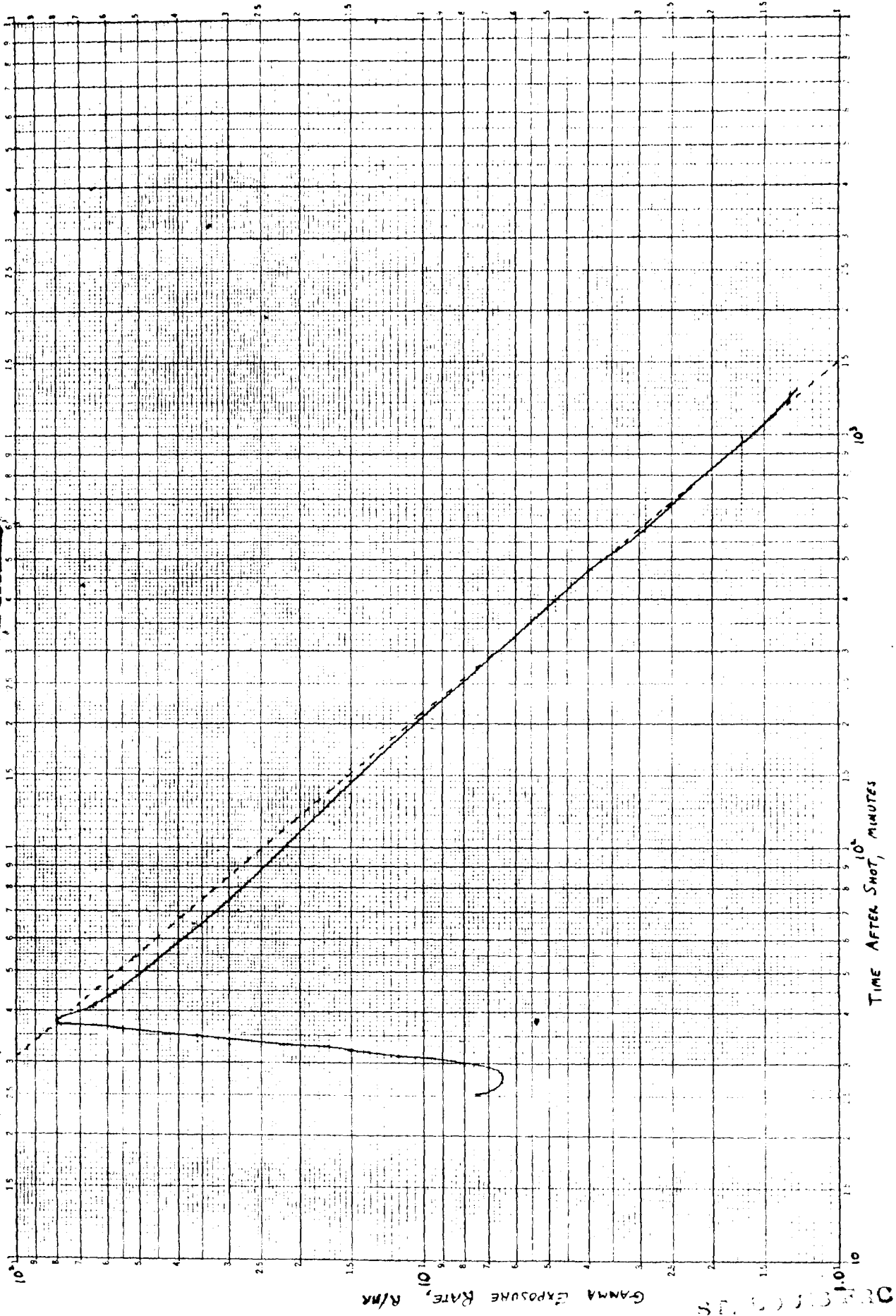
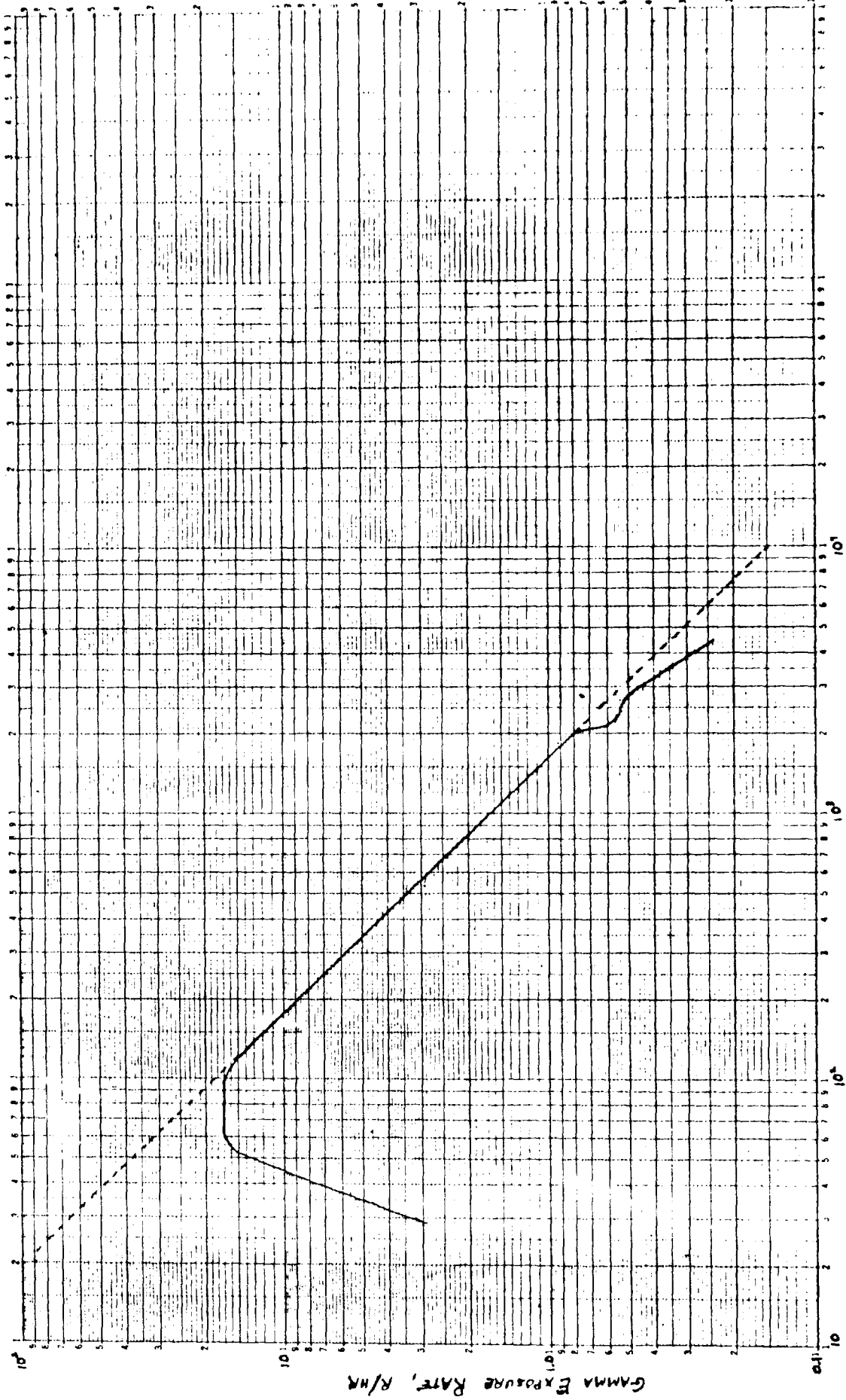


Figure 3.4 Unshielded residual exposure rate versus time for Zuni; Station 221.020, Range 43,400 feet. Total 26.4-hour exposure, 125r.

RESTRICTED DATA  
~~ATOMIC ENERGY ACT OF 1954~~

~~SECRET~~



TIME AFTER SWOT, MINUTES

Figure 3.5 Unshielded residual exposure rate versus time for Zuni; Station Hov, range 78,000 feet.  
Total 74.5-hour exposure, 126r.

~~RESTRICTED DATA  
ATOMIC ENERGY ACT 1954~~

~~SECRET~~

[REDACTED]

DELETED

Station 221-01, Range 45,800 feet.  
Time After Shot, MINUTES  
Figure 3.6 Unshielded residual exposure rate versus time for Flathead; Station 221-01, Range 45,800 feet.  
Total 74.3-hour exposure, [REDACTED]

~~RESTRICTED INFORMATION ACT 1954~~

[REDACTED]

DELETED

ST LOUIS ARC

[REDACTED]

DELETED

Figure 3.7 Residual exposure rate within blast shield versus time for Flathead, Station 221.04, range 7,730 feet. For unshielded rate, multiply by 1.4. Total 52.3-hour exposure [REDACTED]

DELETED  
EXCLUDED DATA  
APR 1954

[REDACTED]

ST. LOUIS MO

15



[REDACTED]

DELETED

7

Figure 3.9 Residual exposure rate within blast shield versus time for Flathead; Station 201.08 (detector inside steel pipe), range 14.94 feet. For unshielded rate, multiply by 1.4. Total 37.6-hour exposure, [REDACTED]

DELETED

ST. LOUIS WRC

RESTRICTED DATA  
ATOMIC ENERGY ACT

[REDACTED]

52

53

[REDACTED]

DELETED

TIME AFTER SHOT, MINUTES

Figure 3.10 Unshielded residual exposure rate versus time for Featherhead; Station 221.06 (detector outside steel pipe), range 14,920 feet. Total 51-hour exposure

RESTRICTED BY ACT 1954

ST. LOUIS MO

[REDACTED]

DELETED

Time After Shot, minutes

Figure 3.11 Unshielded residual exposure rate versus time for Flathead; Station 221.04C, range 70,000 feet. Total 85-hour exposure, [REDACTED]

DELETED

~~RESIDUAL EXPOSURE RATE~~

[REDACTED]

[REDACTED]

DELETED

ST. LOUIS FRC

Time After Shot, minutes

Figure 3.12 Unshielded residual exposure rate versus time for Navajo; Station 221.01, range 46,300 feet. Total 50-hour exposure, [REDACTED]

DELETED

11

~~CONFIDENTIAL - SECURITY ACT 1954~~

[REDACTED]

[REDACTED]

DELETED

Figure 3.1.3 Residual exposure rate within blast shield versus time for Navajoj Station 221.03, range 7,922 feet. For unshielded rate, multiply by 1.4. Total 53-hour exposure [REDACTED]

RESTRICTED DATA  
~~ATOMIC ENERGY ACT 1954~~

[REDACTED]

[REDACTED]

DELETED

7

ST. LOUIS WAC

Figure 3.14. Residual exposure rate within blast shield versus time for Navajo; Station 221.04, range 700 feet. For unshielded rate, multiply by 1.4. Total 47-hour exposure, [REDACTED]

DELETED

~~CONFIDENTIAL~~  
~~PERMIT ACT 1954~~

[REDACTED]

~~SECRET~~

TIME AFTER SHOT, MINUTES

Station 22L.05, range 13,170

Figure 3.15 Residual exposure rate within blast shield versus time for Navajo; Total 37-hour exposure, feet. For unshielded rate, multiply by 1.4.

~~SECRET~~

~~SECRET DATA~~

~~SECRET~~

ST. LOUIS HQ

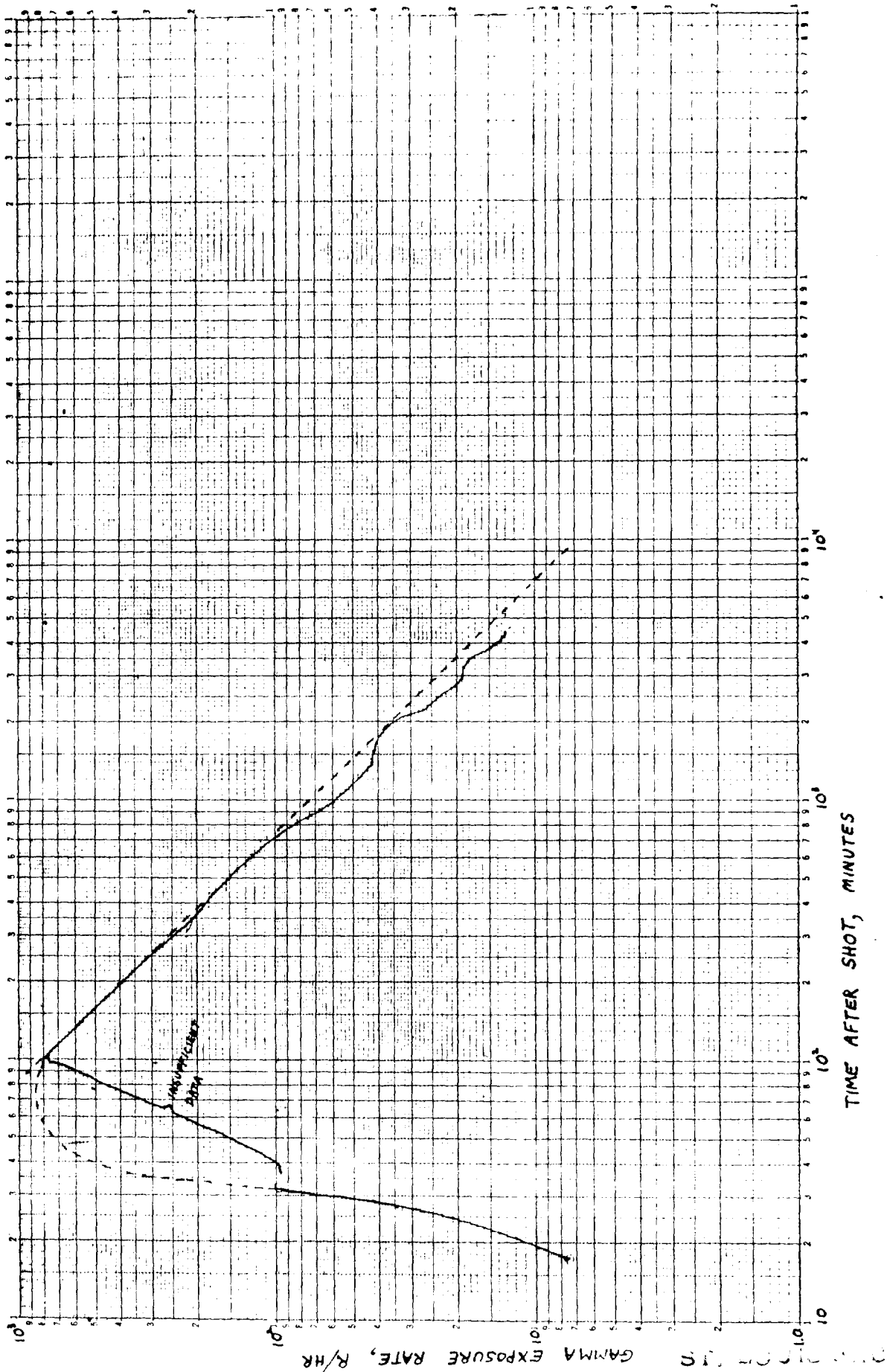


Figure 3.16 Residual exposure rate versus time for Teva; Station 221.01, range 28,950 feet. For unshielded rate, multiply by 1.4. Total 74.8-hour exposure, 3055rA

~~UNCLASSIFIED DATA~~  
~~RESIDUAL EXPOSURE RATE~~

~~SECRET~~

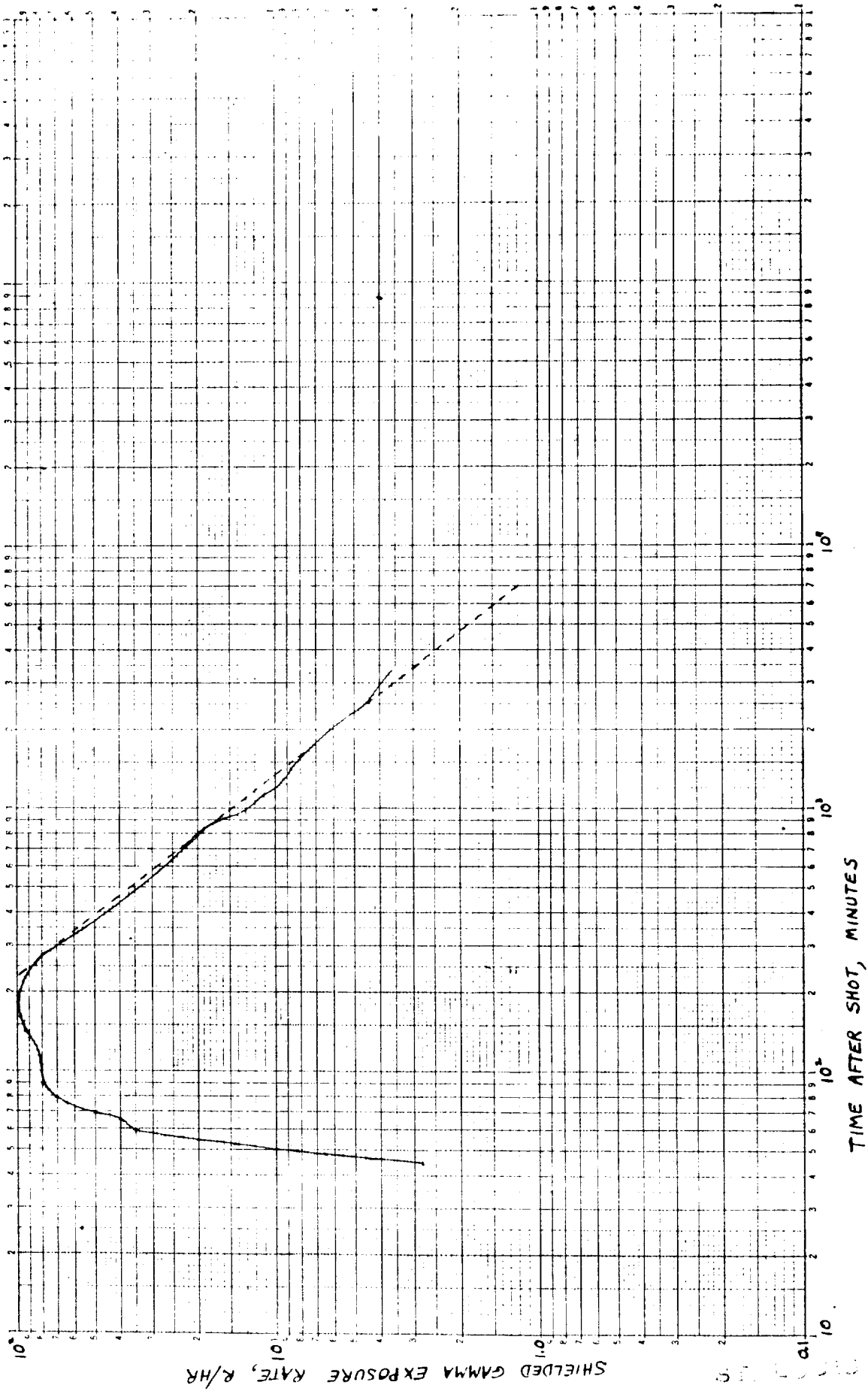


Figure 3.17 Residual exposure rate within blast shield versus time for Teva; Station 221.03, range 17.550 feet. For unshielded rate, multiply by 1.4. Total 55-hour exposure, 948r.

~~RESIDUAL GAMMA EXPOSURE RATE~~  
~~ATOMIC ENERGY~~

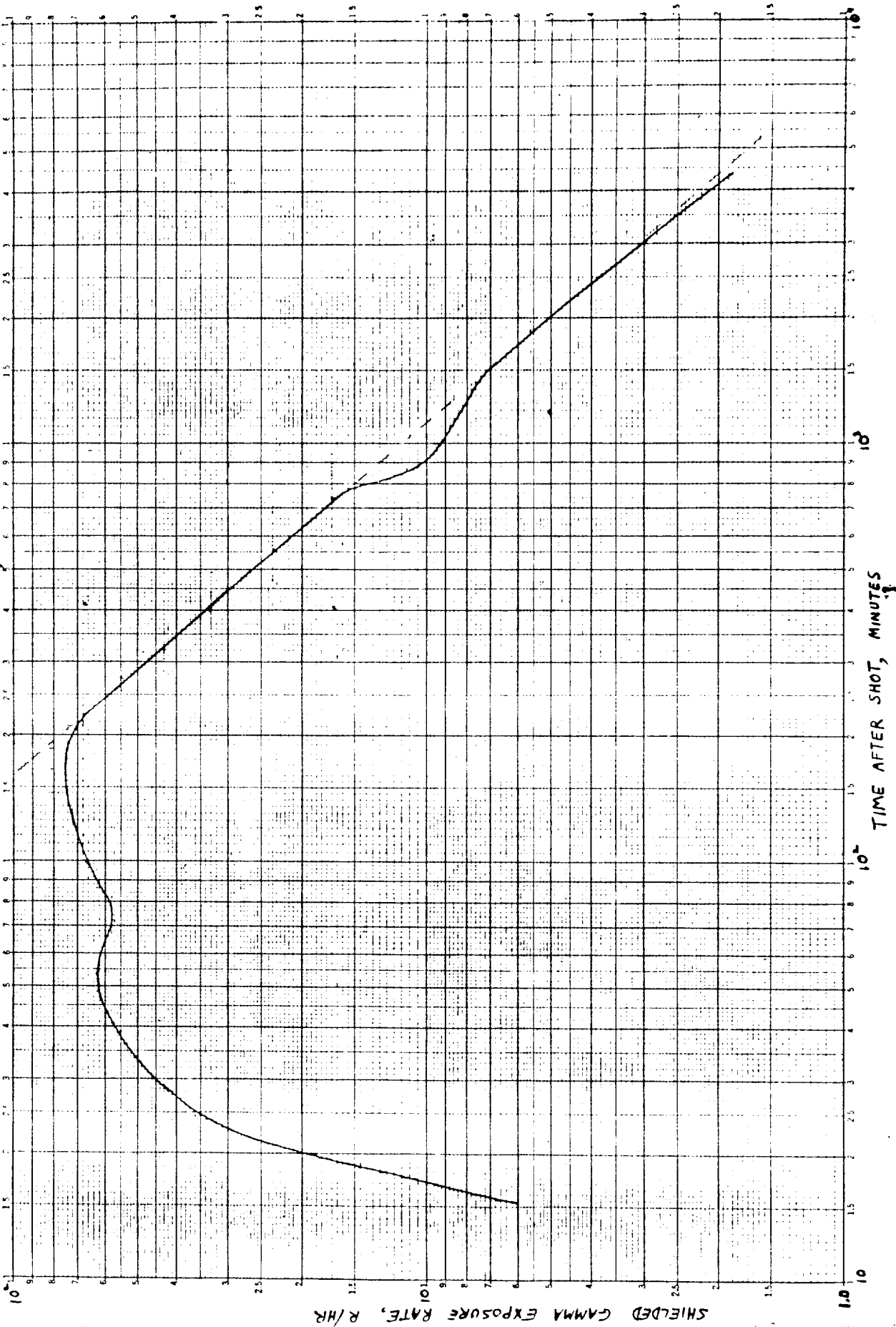


Figure 3.18 Residual exposure rate within blast shield versus time for Tewa; Station 221.04, range 22,220 feet. For unshielded rate, multiply by 1.4. Total 73-hour exposure, 814r.

~~RESTRICTED DATA  
ATOMIC ENERGY ACT 1954~~

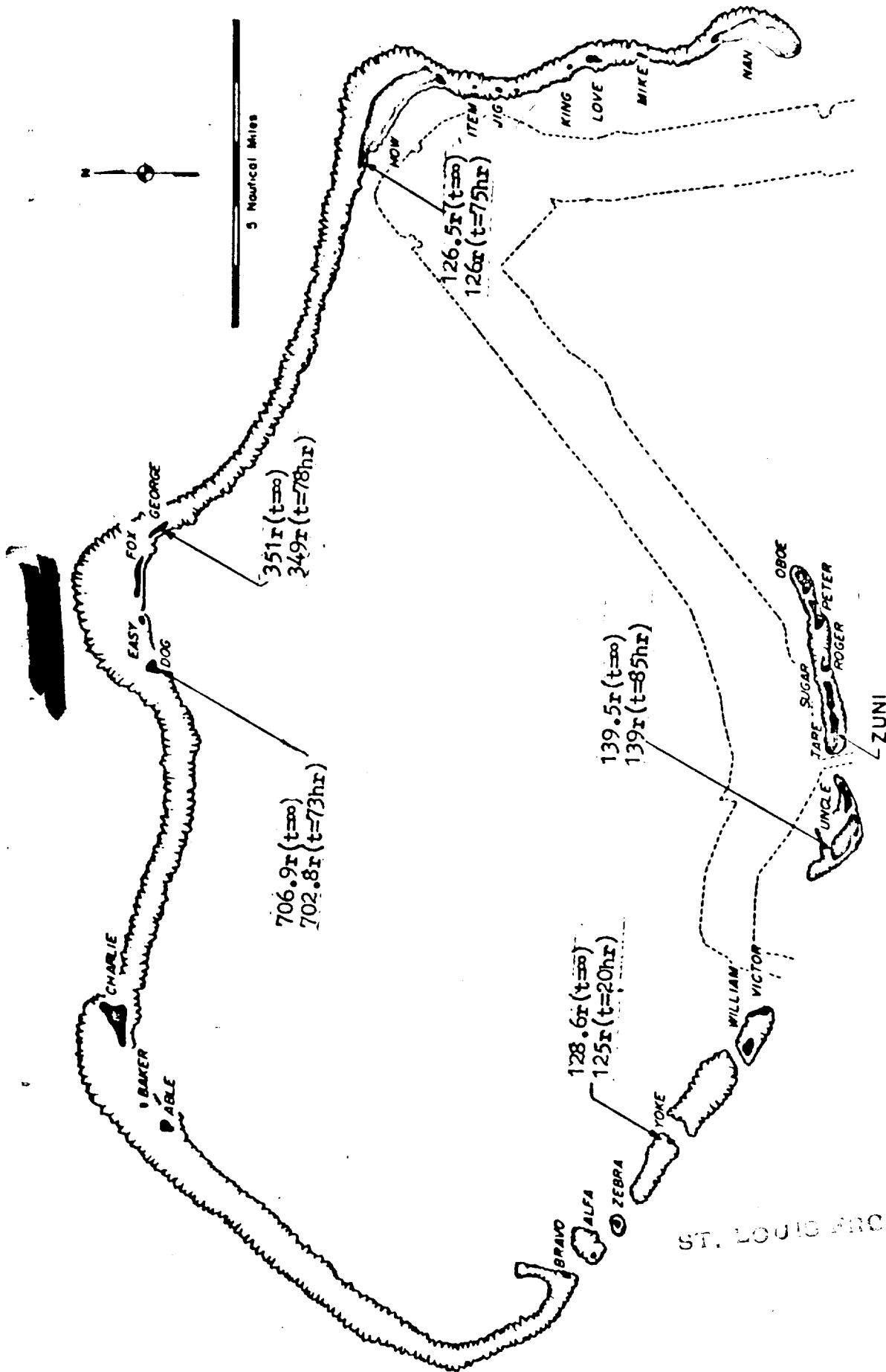


Figure 3.19 Map of Bikini Atoll showing unshielded residual exposures for Shot Zuni. This illustration gives exposures at Islands Dog, George, How, Uncle, and Yoke. See Table 3.1 for references to station designations, distances from GZ, arrival times, and maximum exposure rates.

~~RESTRICTED DATA~~  
~~ATOMIC ENERGY ACT 1054~~

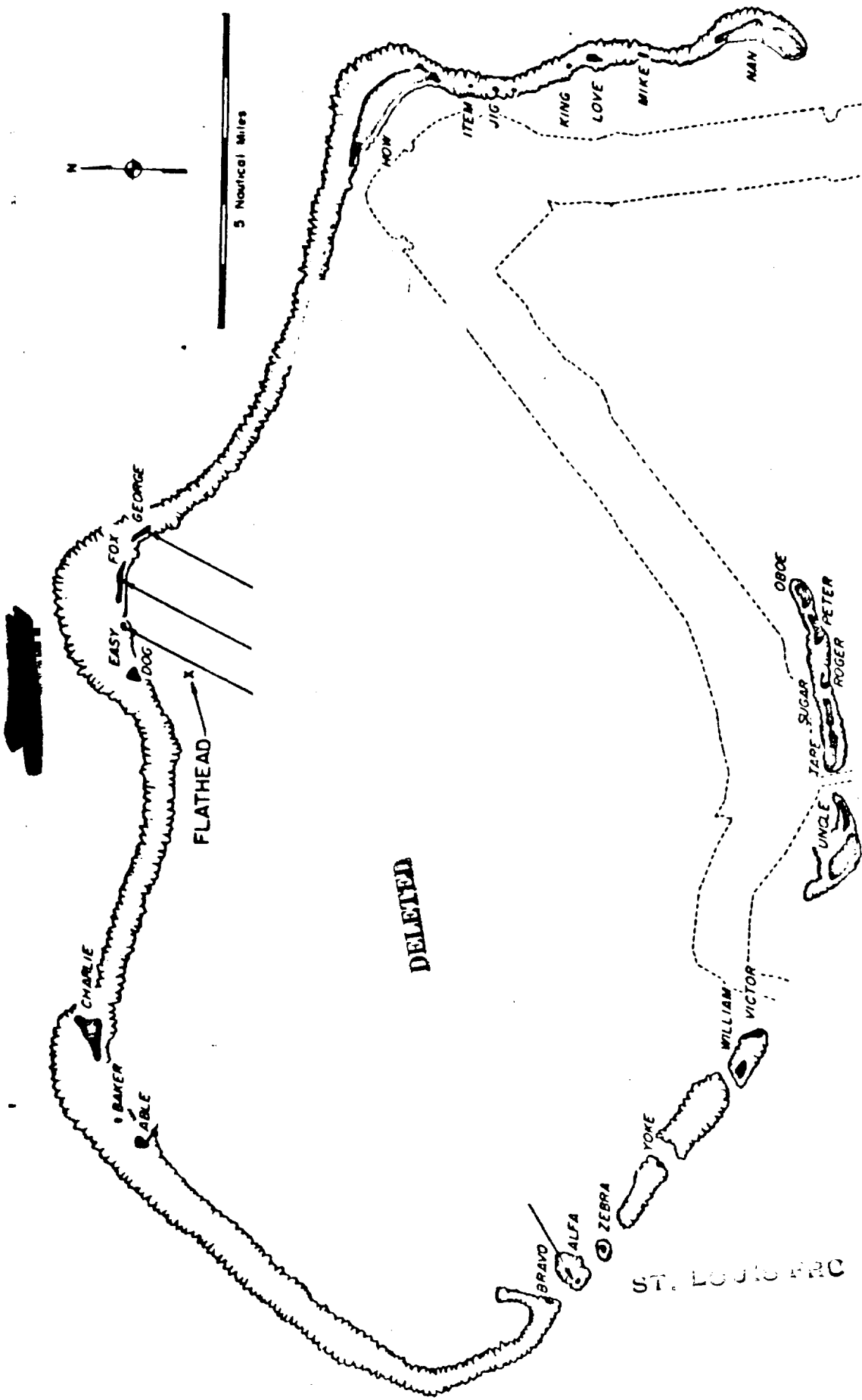


Figure 3.20 Map of Bikini Atoll showing unshielded residual exposures for Shot Flathead. This illustration gives exposures at islands Able, Alfa, Easy, Fox, and George (a and b). See Table 3.2 for references to station designations, distances from GZ, arrival times, and maximum exposure rates.

~~RESTRICTED DATA~~

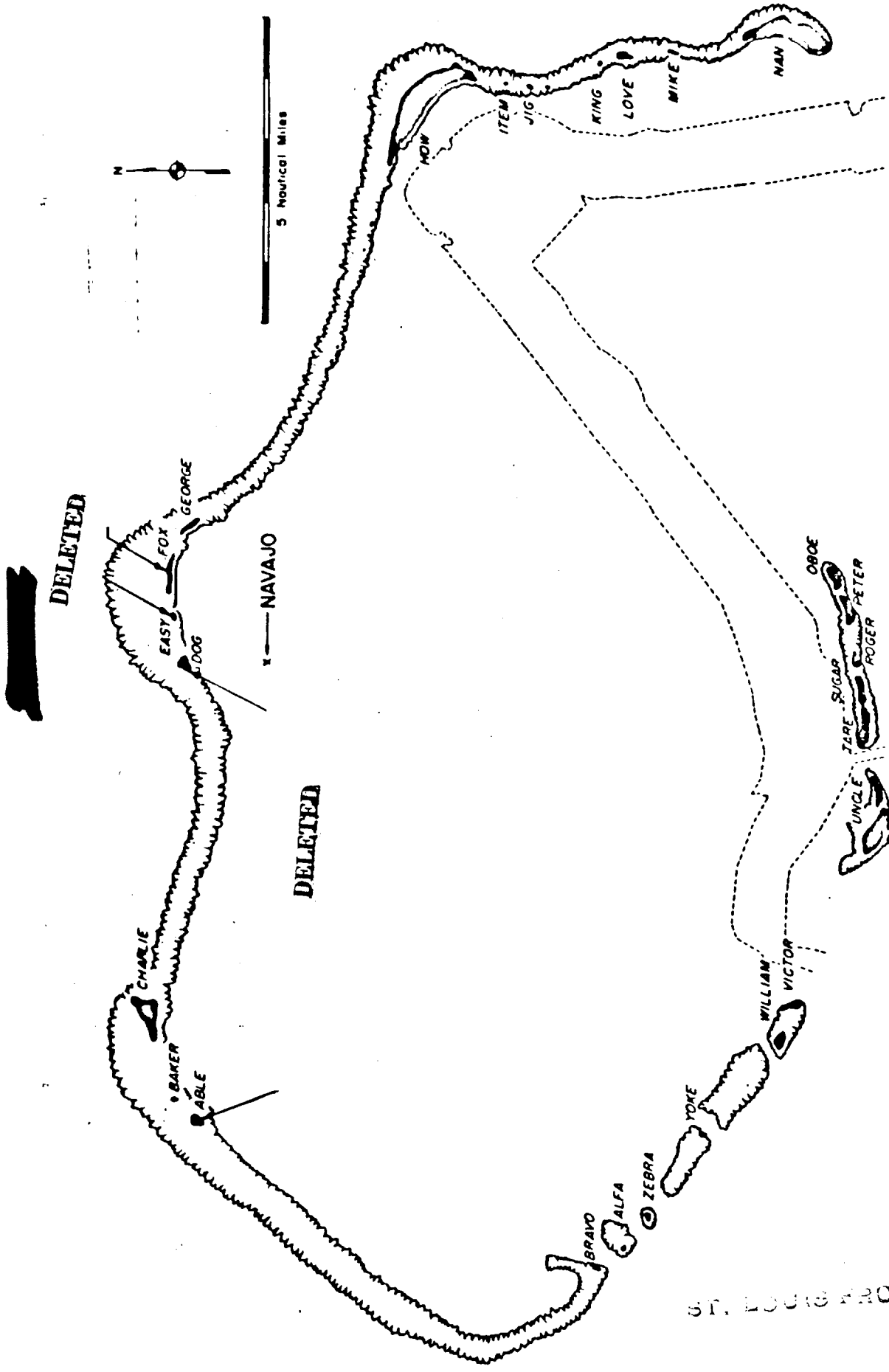


Figure 3.21 Map of Bikini Atoll showing unshielded residual exposures for Shot Navajo. This illustration gives exposures at Islands Able, Dog, Easy, and Fox. See Table 3.3 for references to station designations, distances from GZ, arrival times, and maximum exposure rates.

~~UNCLASSIFIED DATA  
ALCANTARA PERSONNEL ACT 1954~~

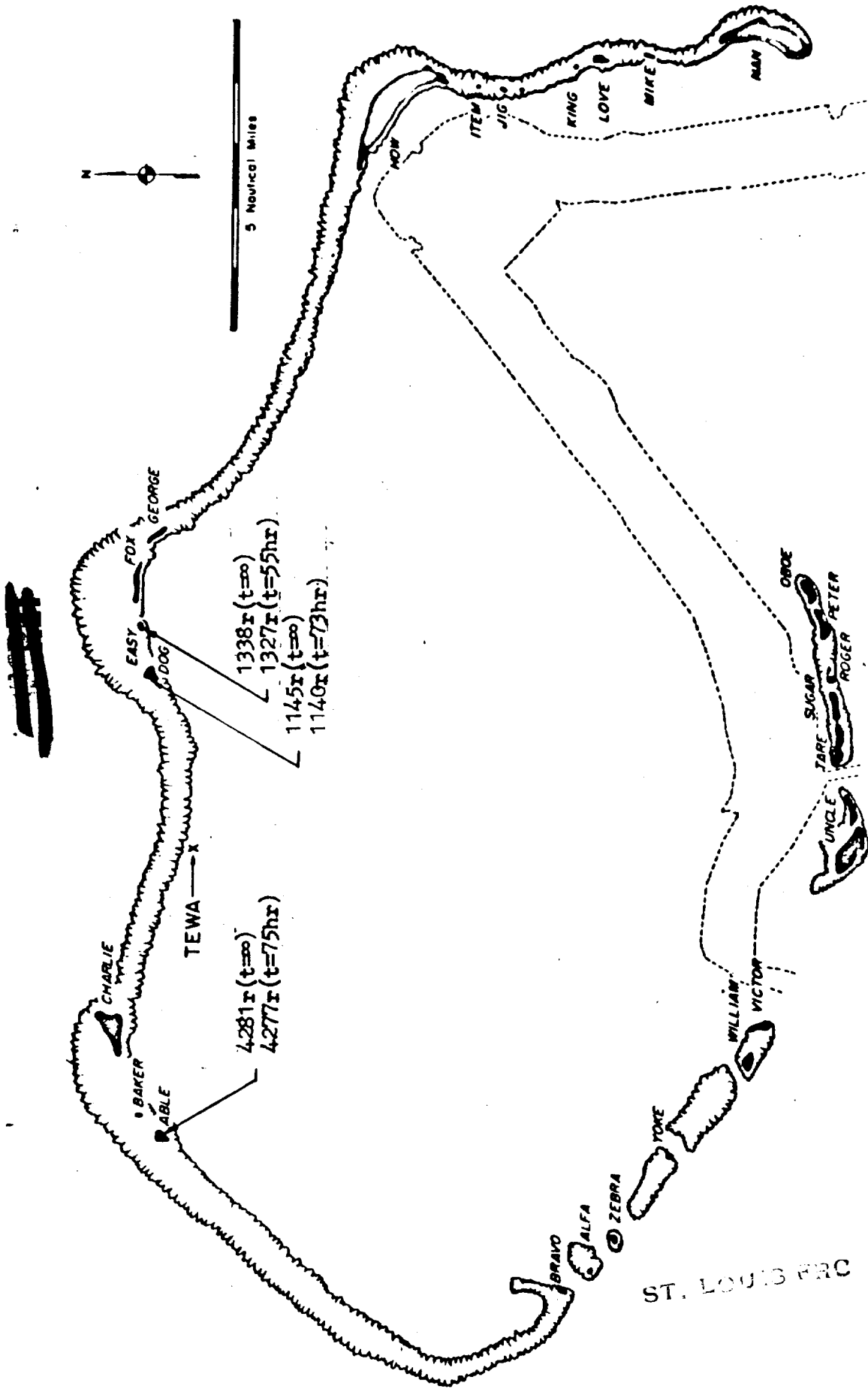
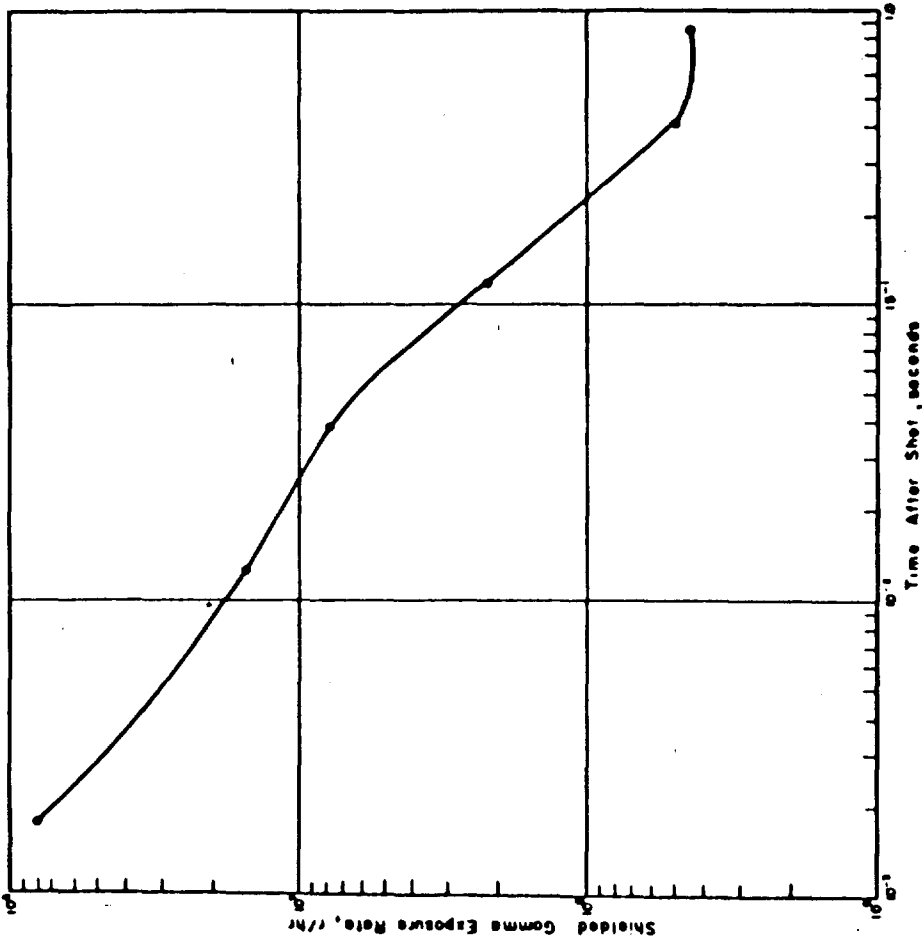


Figure 3.22 Map of Bikini Atoll showing residual exposures for Shot Teva. This illustration gives exposures at Islands Able, Dog, and Easy. See Table 3.4 for references to station designations, distances from GZ, arrival times, and maximum exposure rates.

~~SECRET~~  
 1054



ST. LOUIS AEC

Figure 3.23 Shielded initial exposure rate versus time for Zuni; Station 220,09C, range 7,000 feet. For unshielded rate multiply by 1.2.

RESTRICTED DATA  
 ATOMICS ENERGY COM. 4054

[REDACTED]

**DELETED**

Figure 3.24 Shielded initial exposure rate versus time for Flathead; Station 221.04, range 7,730 feet. For unshielded rate multiply by 1.2.

RESTRICTED DATA  
~~ATOMIC ENERGY ACT 1954~~

[REDACTED]

[REDACTED]

**DELETED**

Figure 3.25 Shielded initial exposure rate within blast shield versus time for Navaajo; Station 221.05, range 13,170-feet. For unshielded rate multiply by 1.2.

[REDACTED] **RESTRICTED DATA**  
**ATOMIC ENERGY ACT 1954**

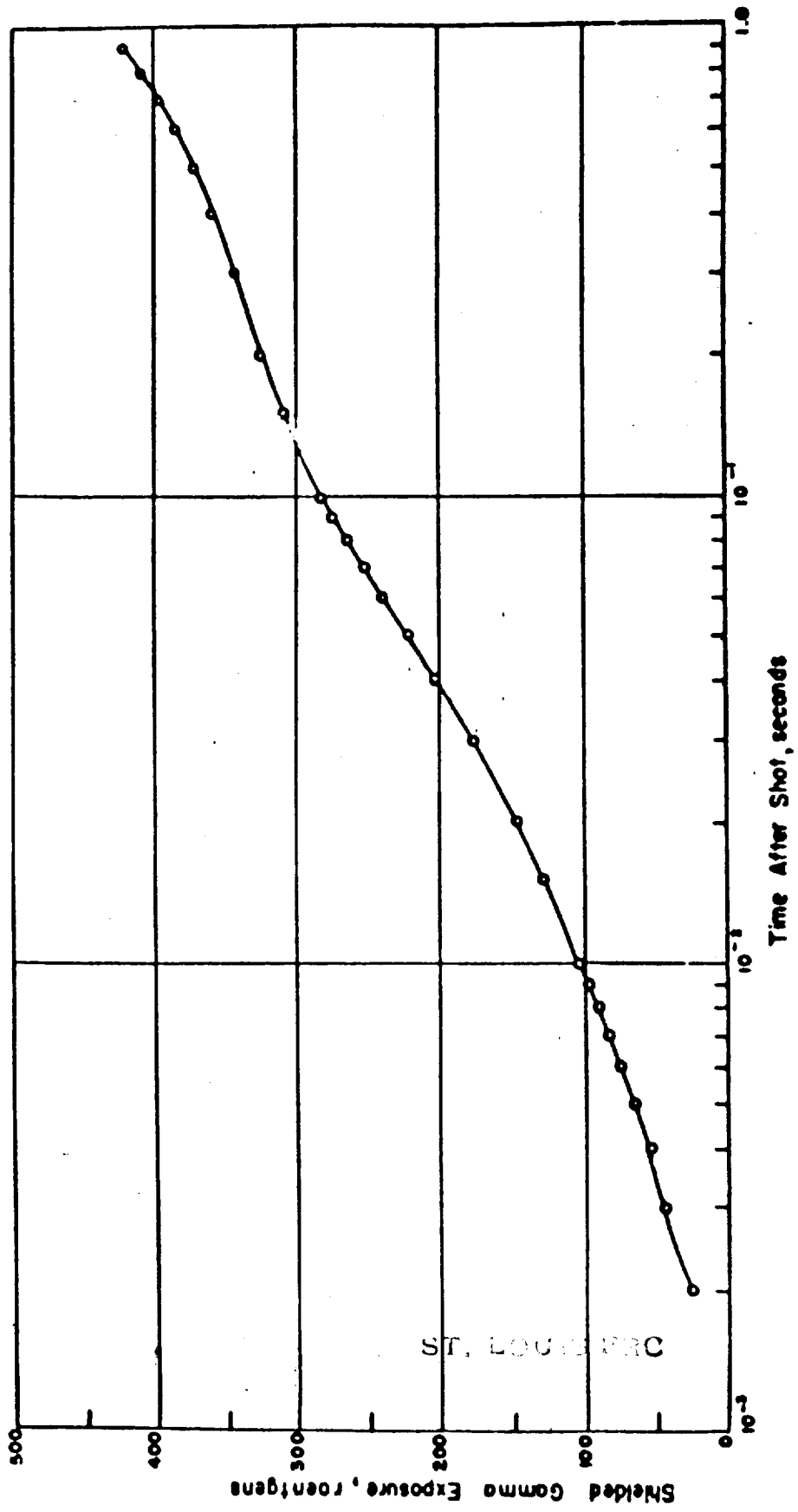


Figure 3.26 Shielded initial exposure versus time for Zuni; Station 220.09C, range 7,000 feet.  
 For unshielded exposure multiply by 1.2.

~~UNPUBLISHED DATA  
 ATOMIC ENERGY COMMISSION  
 OCT. 1954~~

[REDACTED]

**DELETED**

Figure 3.27 Shielded initial exposure versus time for Flathead; Station 221.04, range 7,730 feet. For unshielded exposure multiply by 1.2.

~~RESTRICTED AREA  
ATOMIC ENERGY ACT~~

[REDACTED]

[REDACTED]

**DELETED**

Figure 3.28 Shielded initial exposure versus time for Navajo; Station 221.05, range 13,170 feet. For unshielded exposure multiply by 1.2.

~~RESTRICTED DATA  
ATOMIC ENERGY - 105A~~

[REDACTED]

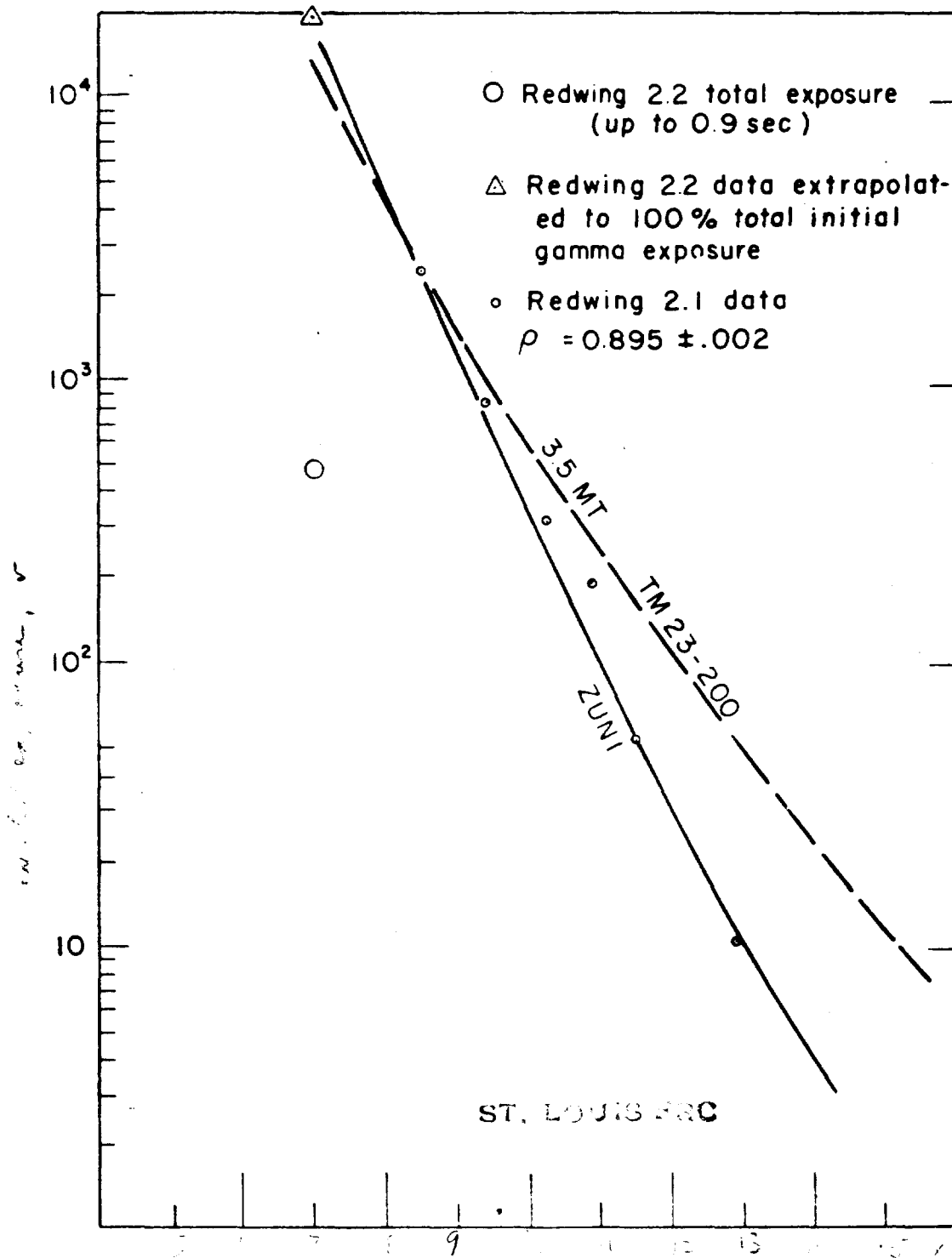


Figure 3.29 Shielded initial exposure versus time, Projects 2.1 and 2.2, Shot Zuni. (Data - see p 73)

~~RESTRICTED DATA~~  
~~ATOMIC ENERGY~~

Initial Exposure, r

**DELETED**

Distance,  $10^3$  feet

73

Figure 1.30 Shielded initial exposure vs.  $1/r^2$ , Projects 2.1 and 2.2, Shots Flathead and Hedwig.  
(Data from Hedwig Project 2.2 plotted on curves presented in Hedwig 2.1 WT report. Reference to

**RESTRICTED DATA**

**PROJECT 2.1**

**PROJECT 2.2**

74

~~SECRET~~

CHAPTER 4

CONCLUSIONS

4.1 RESIDUAL-GAMMA EXPOSURE RATE

The results of the residual-gamma-exposure-rate measurements show that for some devices the decay exponent varies with both the type of device and the station location. The decay exponent was fairly uniform for different station locations for Shot Zuni (1.04 to 1.18) and rather variable for various station locations for Shot Navajo (1.07 to 1.39). Although no special significance is attached, the spread of values for the decay exponent seems to be greater when the average value is high and smaller when the average value is low.

The residual instrumentation system performed at about 50 percent of its capability. This is explained by the failure of the recorders, which were not designed as field instruments and were used because no others were available. There were no known failures of the Conrad detectors.

4.2 INITIAL-GAMMA EXPOSURE RATE

Figures 3.27 and 3.28 show that approximately two-thirds of the total initial-gamma exposure was delivered after the arrival of the shock front. Insufficient initial gamma rate or dose data is available to allow independent comparison with published scaling laws. Figures 3.29 and 3.30 indicate reasonable agreement of both Redwing Projects 2.1 and 2.2 data points with TR 23-200; however, measured dose-versus-distance curves



exhibit a steeper slope than shown on Figure 4-3, page 4-12 of TM 23-200, thus indicating substantial deviations at short and very long ranges.

**4.3 BEACH-BALL OPERATION**

This experiment demonstrated the operational feasibility of using the beach-ball technique to drop a radiological telemeter onto a contaminated area.

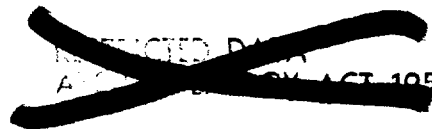
**4.4 THERMAL-RADIATION DETECTOR**

The thermal-radiation detector operated satisfactorily for a 5-Mt detonation at distance of 20 miles.

ST. LOUIS RRC



75



UNCLASSIFIED DATA  
 ACT 1054

76

~~SECRET~~

REFERENCES

1. J. S. Malik; "Gamma Radiation versus Time"; Projects 5.1 and 5.2, Operation Ivy, WT-634, November 1952, Los Alamos Scientific Laboratory; Secret Restricted Data.
2. P. Brown and G. Carp; "Gamma Rate versus Time"; Project 2.2, Operation Castle, ITR-913, May 1954; Evans Signal Laboratory; Secret Restricted Data.
3. Super-Effects Handbook; AFBWP 351, May 1952; Secret Restricted Data.
4. T. E. Petriken; "Evaluation of a Radiological Defense Warning System"; Project 6.1.1b, Operation Teapot, WT-1112, April 1957; Evans Signal Laboratory; Secret Restricted Data.
5. M. G. Schorr and E. S. Gilfillan; "Predicted Scaling of Radiological Effects to Operational Weapons"; Project 2.C, Operation Jangle, WT-391, 15 June 1952; Technical Operations Incorporated; Secret Restricted Data.
6. D. C. Borg and C. M. Eisenhauer; "Spectrum and Attenuation of Initial Gamma Radiation from Nuclear Weapons; AFBWP 502B, January 1955"; Weapons Effects Division; Secret Restricted Data. ST. LOUIS FRC
7. J. S. Malik; "Summary of Information on Gamma Radiation from Atomic Weapons; LA-1620, January 1954; Los Alamos Scientific Laboratory"; Secret Restricted Data.

~~SECRET~~

~~RESTRICTED  
ATOMIC ENERGY ACT 1954~~

[REDACTED]

8. R. T. Carr and G. J. Hine; "Gamma Ray Dosimetry with Organic Scintillators"; *Nucleonics*, November 1953; Unclassified.

9. P. Brown and others; "Gamma Exposure versus Distance"; Project 2.1, Operation Redwing, Draft WF-1310, July 1957; UBASFDL, Fort Monmouth, New Jersey; Secret Restricted Data.

10. "Nuclear Radiation Handbook", AFSWP-1100; 25 March 1957; Nuclear Development Corporation, White Plains, New York; Secret Restricted Data.

ST. LOUIS FRC

7

[REDACTED]

~~RESTRICTED DATA~~

1954

77

78